

Investigating electrodeposition to grow CZTS thin films for solar cell applications

Bachelor Thesis
Pim Reith & Gerben Hopman

Tutor: Dr. O. Islam
Teacher: Prof. Dr. Ir. H. Hilgenkamp
June 21, 2012

Interfaces and Correlated Electron Systems (ICE)
Faculty of Science and Technology
Twente University

Abstract

The search for alternative energy sources has solar energy as one of the primary solutions. Thin film solar cells are a technology that uses less materials, but still keeps or even beats efficiencies of normal silicon solar cells. However, some of the materials used in thin film solar cells are either rare or toxic.

In this project, copper zinc tin sulfide (CZTS) thin films grown on indium tin oxide (ITO) substrates by electrodeposition are investigated as a possible absorber layer in thin film solar cells. The goal is to find out whether electrodeposition followed by a sulfurization step is a good method of growing these films.

Using an electrolyte containing all four elements of CZTS, optimal growth was achieved at potentials between -1.0 and -1.1 V, growing between 40 and 50 minutes. As-deposited films contained no CZTS, but annealing produced islands of stoichiometric CZTS. However, uniform coverage of the substrate was not achieved.

Using an electrolyte containing only copper, zinc and tin, and adding the sulfur through annealing, yielded better results, achieving uniform coverage over almost the entire deposition area. Measurements showed, though, that the annealed film contained too much tin (in the form of tin sulfides), which means the three metals were not deposited in the correct ratios. More research into this method could lead to good results for the electrodeposition of CZTS.

Contents

1	Introduction	1
2	Theory	3
2.1	Semiconductors and pn-junctions	3
2.2	Thin Film Solar Cells	5
2.3	CZTS	7
2.3.1	Secondary phases	8
2.4	Overview of research on CZTS thin film deposition	10
2.4.1	Todorov et al.	10
2.4.2	Katagiri et al.	10
2.4.3	Shin et al.	11
2.5	Alternative solar cell technologies	11
2.5.1	Amorphous and nanocrystalline silicon	11
2.5.2	Cadmium Telluride (CdTe)	12
2.5.3	CIS, CISE and CIGS(e)	12
2.5.4	III-V materials	13
2.5.5	Dye-sensitized solar cells	13
2.5.6	Quantumdot absorber	13
2.5.7	Organic absorbers	14
2.6	Electrodeposition	14
3	Experimental details	17
3.1	Substrate	17
3.2	Deposition parameters	18
3.2.1	Applied voltage	18
3.2.2	pH value	18
3.2.3	Concentration of materials	18
3.2.4	Time	19
3.2.5	Temperature	19
3.2.6	Complexing agent	19
3.3	Deposition	19

3.4	Measuring film properties	20
3.5	Annealing	20
3.6	Cyclic Voltammetry	21
4	Results	23
4.1	What to expect	23
4.2	Optimizing potential with electrolyte 1	24
4.3	XRD and EDX results	24
4.4	Deposition time	25
4.5	XRD, SEM and EDX measurements	26
4.6	Annealing in nitrogen environment	27
4.7	Annealing in sulphur environment	28
4.8	Deposition with electrolyte 2	31
5	Discussion	35
6	Conclusions	39
	Bibliography	40
A	Measuring techniques	46
B	Equipment	53
C	Guide to electrodeposition	55

List of Figures

2.1	Band structure of different types of solids: a) Metals, b) Insulators and c) Semiconductors	4
2.2	Band structure of a pn-junction	4
2.3	Energy band diagram of a CdS/CdTe thin film solar cell	5
2.4	Structure of a thin film solar cell	6
2.5	Tree diagram showing isoelectronic substitutions starting from silicon	7
2.6	Unit cell of CZTS in the kesterite structure	8
2.7	Phase diagram of CZTS	9
2.8	Basic electrodeposition setup with three electrodes	16
3.1	Typical voltammogram for a reversible system at different scan rates	21
4.1	Diffractogram of CZTS on a molybdenum substrate	23
4.2	SEM images of as-deposited and annealed CZTS	24
4.3	XRD measurement of a) CZTS35, b) CZTS36 and c) the substrate (ITO), d) EDX measurement of CZTS35	25
4.4	SEM images of a) CZTS53, b) CZTS54, c) CZTS55 and d) CZTS56	26
4.5	XRD measurement of CZTS55	27
4.6	XRD measurement of an as-deposited sample	27
4.7	SEM images of a) CZTS66 as-deposited and b) annealed at 500°C	29
4.8	XRD measurements of CZTS66 as-deposited and annealed at various temperatures	29
4.9	Low-magnification SEM image of CZTS66 annealed at 500°C	30
4.10	Low-magnification SEM image of CZTS66 annealed at 550°C	30
4.11	Cyclic voltammetry of electrolyte 2	31
4.12	XRD of CZTS80 post-annealing	32
4.13	SEM images of samples grown in electrolyte 2. a) as-deposited and b) post-annealing	32

1. Introduction

Solar energy provides a clean alternative to fossil fuels. Every hour the light that reaches earth from the sun contains enough energy to fuel humanity's needs for a full year [1]. Needless to say, being able to convert only a fraction of the sunlight hitting the planet into electricity would easily supply us with the energy we need for the coming decades.

There are certain requirements to solar cells: high efficiency, low-cost and a short payback time. Solar cells with higher efficiency will require less area to generate sufficient electricity, and low costs will make solar cells attractive to both producer and customer. A short payback time means they need to win back production costs and energy as quickly as possible.

The current commercial market for solar cells is dominated by cells made of crystalline silicon, accounting for around 80% of the market share [2]. The price of these solar cells is mainly set by the 250-300 μm thick silicon wafer that forms the bulk of the cell. Making the production process cheaper or developing solar cells that require less material to make will reduce costs. One of the alternatives using less material is the thin film solar cell [3].

The downside of this technology, however, is that most of the thin film solar cells are made of rare (and thus expensive) and/or toxic materials. Examples include rare tellurium or indium [4], and the toxic cadmium or selenium [5]. Current thin film solar cells with high efficiencies are based on these materials, but due to the rarity or toxicity of these materials, alternatives are needed.

Copper zinc tin sulfide, commonly known as CZTS, is one of these alternatives. With a band gap of around 1.5 electronvolt [6] and an absorption coefficient of order 10^4 cm^{-1} [6], CZTS is an ideal candidate to be used as an absorber layer in thin film solar cells. The four elements are all highly available in the earth's crust [4] and non-toxic [5].

The goal of this project is to grow stoichiometric films of CZTS using electrodeposition, an easy and cheap deposition method which can be done without vacuum and at room temperature, and can scale to industrial standards [7]. For this, two methods were employed. In the first, the electrolyte contained all four components of CZTS. After deposition, an annealing step

was performed to improve crystallinity and, if needed, incorporate more sulfur. In the second method, the electrolyte did not contain sulfur. The sulfur was added during the annealing process.

This report will investigate and compare the two growth methods and see which one leads to better results. This includes stoichiometry, coverage of the substrate, film uniformity and crystallinity. In addition, a literature study of other types of solar cells has been included.

2. Theory

This chapter will discuss various theoretical aspects of the project. First, some basic semiconductor physics necessary to understand the working principles of solar cells will be given. After that, properties of CZTS and possible secondary phases which can influence film characteristics will be discussed, including some information about some of the bigger research groups. An overview of other solar cell technologies follows after that. The last section will contain some basic theory of electrodeposition.

2.1 Semiconductors and pn-junctions

In solid state physics, materials are categorized based on their electronic band structure. Metals have a band which is partly filled with electrons, which gives them good conducting properties. Semiconductors and insulators, on the other hand, have bands which are either fully occupied or unoccupied. The difference between insulators and semiconductors lies in the energy band gap between the highest filled band (valence band) and the lowest unfilled band (conduction band). Insulators have a large band gap, typically 5 to 10 electronvolt (eV), semiconductors have a smaller band gap, usually around 1 eV [8]. Figure 2.1 shows this categorization schematically.

Semiconductors have electrical properties in between those of metals and those of insulators. However, by adding atoms with a different amount of valence electrons to a semiconductor, the electrical properties can be changed. This process is called doping. Adding an atom which has more valence electrons than the original material (a donor), is called n-type doping (n for negative), due to the surplus of electrons available. Adding an atom with less valence electrons (an acceptor), will create vacant states, commonly known as holes, and is therefore called p-type doping (p for positive).

Doping a semiconductor changes the Fermi energy. Normally it is located halfway between the valence band and the conduction band. In a p-type semiconductor, the Fermi energy is lowered, while the opposite holds for n-type semiconductors. This change in Fermi energy plays an important role

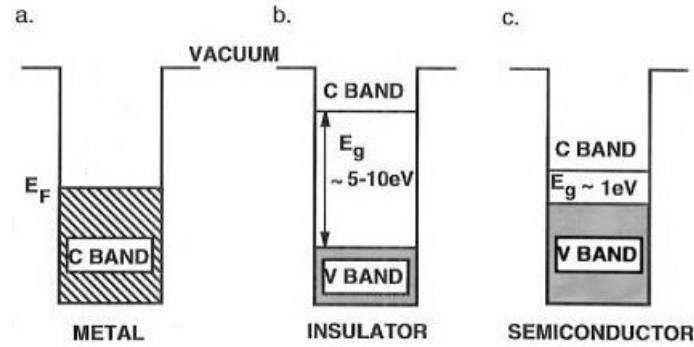


Figure 2.1: Band structure of different types of solids: a) Metals, b) Insulators and c) Semiconductors. E_g is the energy band gap between the valence band (V band) and the conduction band (C band). Adapted from [8].

in semiconductor devices like solar cells.

By combining a p-type material with an n-type material, the interface becomes a so-called pn-junction. For any solid in equilibrium, the Fermi level must be the same everywhere. Since p-type and n-type materials have different Fermi levels, they need to be matched by bending the band structure. This band bending can be seen in Figure 2.2.

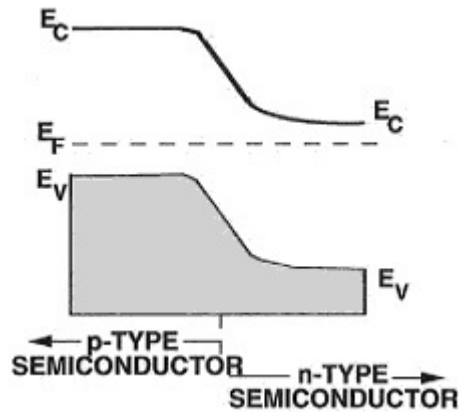


Figure 2.2: Band structure of a pn-junction [8].

Band bending is caused by electrons from the n-type material diffusing into the p-type material, leaving behind positively charged ions, while holes from the p-type material will move into the n-type material, leaving behind negatively charged ions. These ions in turn will create a built-in electric field that opposes the diffusion process, eventually creating equilibrium between the two.

Solar cells are based on pn-junctions to create electricity using incoming light. When a photon is absorbed by an electron, the electron is excited across the band gap into the conduction band, leaving behind a hole. The electron and hole are called an electron-hole pair, or exciton. Due to the band structure of a pn-junction, the electron will move into the n-type material, while the hole will move into the p-type material, creating an electrical current (see Figure 2.3). This process is called the photovoltaic effect and forms the basis of all solar cells.

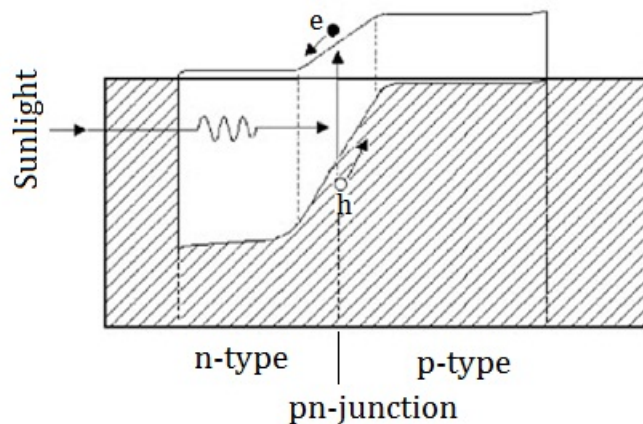


Figure 2.3: Energy band diagram of a CdS/CdTe thin film solar cell, illustrating the basic idea behind the photovoltaic effect. Incident sunlight creates an electron (e) - hole (h) pair, which flow in opposite directions to create a current. Adapted from [9].

During production, defects can occur in the semiconductor material. Defects can be dislocations, misfits with the substrate (i.e., the lattice parameters of the substrate and film do not match) or secondary crystal phases. Defects reduce the mobility of charge carriers, which means they recombine faster with a hole, thereby reducing the current.

2.2 Thin Film Solar Cells

Thin film solar cells are a developing technology based on, as the name suggests, thin layers (thickness in the order of μm) of specialized materials to create the photovoltaic effect. The different layers, as can be seen in Figure 2.4, perform different functions in the solar cell.

The top layer is a transparent conducting layer, usually made of zinc oxide or indium tin oxide (also known as ITO). This layer acts as one of the two contact points of the solar cell, and is optically transparent to make sure

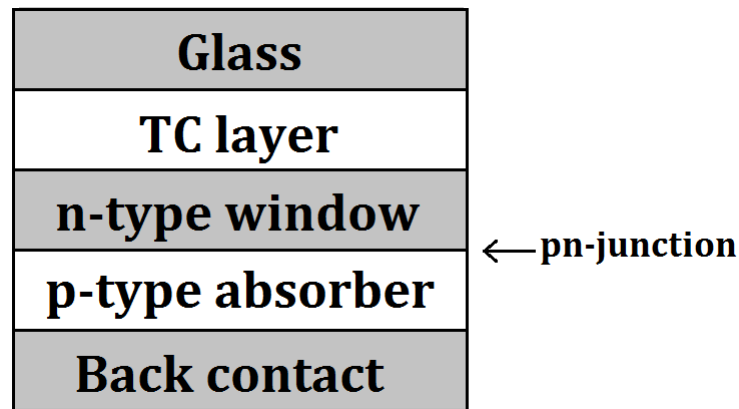


Figure 2.4: Structure of a thin film solar cell. 'TC layer' stands for 'transparent conducting layer'.

the sunlight passes through. The bottom layer, the back contact, serves as the other contact point.

The most important role is played by two layers of semiconducting material: the "absorber" layer and the "window" layer. The absorber layer is a p-type semiconductor with a band gap ideally around 1.4 eV. This is based on the Shockley-Queisser limit, which predicts a maximal theoretical efficiency of a single-junction solar cell [10]. The window layer is an n-type material with a large band gap (for example, the commonly used cadmium sulfide has a band gap of 2.42 eV [9]) to prevent it from absorbing incoming photons. The function of the window layer is purely to create the pn-junction required for the photovoltaic effect.

One of the currently leading types of thin film solar cell uses an absorber layer of copper indium gallium sulfide/selenide (CIGS), with a 2010 thin film solar cell market share of 25% [2]. This type of solar cell has achieved efficiencies of 20% [11]. However, CIGS cells use indium and gallium, metals which are rare in the earth's crust and therefore either expensive or predicted to become expensive in the near future [4].

Another type of solar cell is the cadmium telluride (CdTe) solar cell, which had a 2010 market share of 43% [2] and has reached efficiencies of 16.7% [11]. As with the indium and gallium in the CIGS solar cell, however, tellurium is a rare metal [4]. Additionally, cadmium is a highly toxic material [5], making production of cells using cadmium require strict working conditions.

Since these solar cells, and other thin film solar cells like them, require either rare or toxic materials, the goal is to find replacements that are made out of safe and abundantly available materials. One such replacement is copper zinc tin sulfide, also known as CZTS.

2.3 CZTS

Semiconductor compounds can be derived from existing semiconductors by isoelectronic substitution. Two atoms or molecules are isoelectronic if they have the same amount of valence electrons. For example, a pair of silicon atoms is isoelectronic with gallium arsenide. Figure 2.5 shows how various semiconductors can be obtained starting from silicon using isoelectronic substitution.

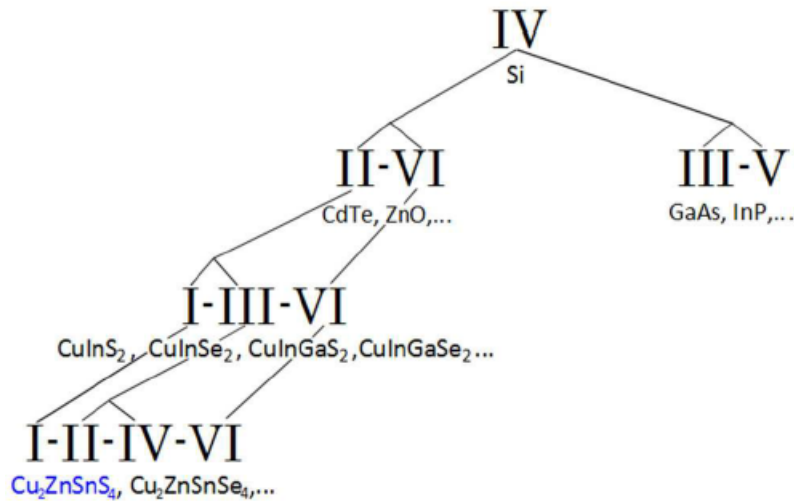


Figure 2.5: Tree diagram showing isoelectronic substitutions starting from silicon. The roman numerals indicate the group number on the periodic table. CZTS is highlighted in blue. [12]

In an attempt to replace rare or toxic elements in a compound, isoelectronic alterations can be made to obtain a new compound with the same electronic structure. Taking CIGS, indium and gallium (both group III elements) can be replaced using a group II and a group IV element. Since the goal is to use non-toxic and abundant materials, tin and zinc are good candidates [4, 5]. Replacing selenium with sulfur (which are from the same group) turns CIGS into CZTS.

CZTS ($\text{Cu}_2\text{ZnSnS}_4$) is a crystal that forms in the kesterite structure, shown in Figure 2.6. The kesterite structure is a tetragonal crystal structure with lattice parameters of $a = 5.434$ ångström (Å , 10^{-10} m) and $c = 10.856$ Å [14]. CZTS has an absorption coefficient in the order of 10^4 cm^{-1} [15] and a direct energy band gap of around 1.5 eV at room temperature [6, 16], properties which make it a suitable candidate to replace CIGS as an absorber layer in thin film solar cells. Another property that strengthens this claim is that CZTS, like CIGS, is a p-type semiconductor. This is due to an intrinsic

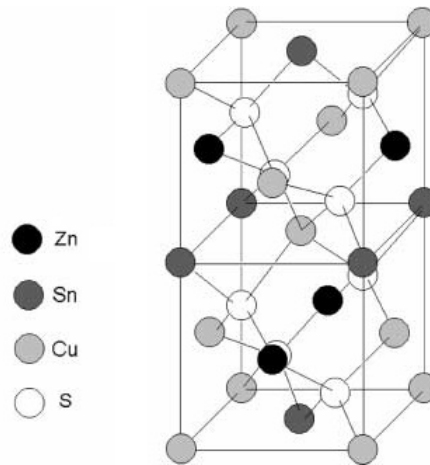


Figure 2.6: Unit cell of CZTS in the kesterite structure. Adapted from [13]

defect, where a copper atom sits on a zinc site [17]. This means that the established thin film solar cell structure can be adopted, with CZTS as the absorber layer instead of CIGS.

2.3.1 Secondary phases

Secondary phases are substances in the film that are not CZTS, but are a compound of one or more of its constituents. They occur when there is a surplus of certain materials that remain after the rest has formed into CZTS, or before CZTS has fully formed. The phase diagram in Figure 2.7 shows when certain secondary phases appear.

Some secondary phases alter the properties of the film in a detrimental way, such as promoting recombination or adding insulating regions. These secondary phases will be discussed here.

Copper sulfides

Copper sulfides are, or behave like, metals, which means they are good conductors. Large crystals can shunt the solar cell, connecting the front and back electrode. This means the solar cell cannot be used for an external load. Smaller crystals, although they do not shunt the cell, enhance recombination, reducing the current [12].

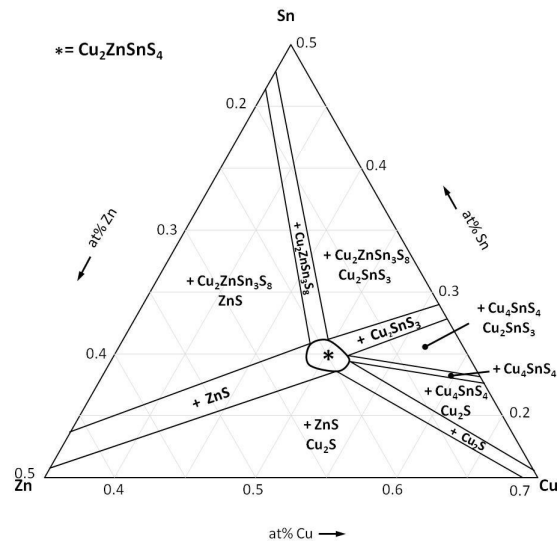


Figure 2.7: Phase diagram of CZTS. This phase diagram assumes 50% sulfur [18].

Tin(IV) sulfide

Tin(IV) sulfide (SnS_2) is an n-type semiconductor with a band gap of 2.2 eV [19]. This means that in large amounts, the tin sulfide could create a diode of opposite polarity to CZTS, forming an electrical barrier. In smaller amounts it can act as an insulating phase, also reducing electrical properties and limiting the area where electron-hole pairs will form [12].

Zinc sulfide

Zinc sulfide (ZnS) has a large band gap of 3.5-3.8 eV [20], which makes it behave like an insulator. As before, insulating phases reduce electrical properties as well as reducing the area where electron-hole pairs can be formed. Additionally, one possible crystal structure of zinc sulfide (sphalerite) is similar to that of CZTS, which means they share some peaks in XRD measurements. This makes it harder to determine if zinc sulfide phases are present [12].

Copper tin sulfide

Copper tin sulfide (Cu_2SnS_3 or CTS) has metallic properties, similar to copper sulfide [21]. This can cause shunts in the solar cell, or enhance recombination in smaller amounts. Like zinc sulfide, CTS shares peaks with CZTS in XRD measurements, making it difficult to detect [12].

2.4 Overview of research on CZTS thin film deposition

Various other groups have done research on depositing CZTS thin films using different deposition methods. An overview can be found in the paper *Progress in Thin Film Solar Cells Based on Cu_2ZnSnS_4* by H. Wang [22], which details a lot of research groups and their progress. A few of the most notable groups will be highlighted in this section. The most important player in the field is IBM, which has several groups working on different methods of creating CZTS thin films. Typical result range between 5% and 7% efficiency, with 10.1% as the current record. AQT Solar, a leading CIGS solar cell production company, have made a 60 watt CZTS solar cell panel prototype, and are hoping to commercialize CZTS solar cells in 2013 [23].

2.4.1 Todorov et al.

Todorov et al., based at IBM in the US, have thus far achieved the highest conversion with a solar cell based on CZTS, being 10.1% [24]. They deposited films using an ink-based method using hydrazine as the solvent. By spin coating the ink on the surface and evaporating the solvent, CZTS is deposited as a thin film. Although the results seem commercially viable, the problem lies with hydrazine. As explained earlier, hydrazine is highly unstable and must be handled using very strict protocols.

Todorov et al. are working on an aqueous-based solution to replace the hydrazine, and have reported a conversion efficiency of 8.1% using CZTS films deposited in this fashion [25].

2.4.2 Katagiri et al.

Katagiri's group, from Nagaoka National College of Technology in Japan, has been working on CZTS solar cells since the nineties. This group deposited films by co-sputtering copper, zinc sulfide and tin sulfide targets, which were then annealed in a sulfur environment. Devices created in this way reached an efficiency of 6.7% [26]. Aside from the lower efficiency, sputtering is also a vacuum-based method, which makes production on a large scale complicated. This is in contrast to Todorovs group, whose method of ink-based solutions is already widely applied in industry.

Katagiri et al. also attempted co-evaporation of the different components of CZTS, achieving an efficiency of 5.7%, but no progress on this has been reported other than the initial paper from 2008 [26,27].

2.4.3 Shin et al.

Shin et al. from IBM used thermal evaporation of zinc, tin, copper and sulfur sources, followed by a short annealing step (5 minutes at 570°C) to grow CZTS films. Devices created from this reached efficiencies up to 8.4% [7]. This is again a method using a vacuum environment, making it less attractive for mass production.

2.5 Alternative solar cell technologies

This section will try to give an overview of alternatives to the crystalline silicon absorber layer. Some of these are already used commercially and research is focused on improving the efficiency and/or reducing the production cost. Other absorber layers have thus far only been made in laboratories. One must keep in mind that it is hard to compare these materials, since the device structure can be entirely different, using for example a single-junction structure instead of a multi-junction structure, different window layers or contacts.

Three types of thin film solar cells have been commercially used thus far. These are the hydrogenated amorphous silicon (a-Si:H), the CdTe and the CIGS solar cell.

2.5.1 Amorphous and nanocrystalline silicon

Amorphous silicon (a-Si) is a widely used material for thin film solar cells because it is abundant and non-toxic, requires low temperature processing, the technological capability for large-area deposition exists and the material requirements are much lower (1-2 μm layer thickness) due to the high absorption compared to crystalline silicon. The material has a high defect density, which causes more optical transitions to be possible, but defects also serve as a centre of recombination [3].

By incorporating around 10% hydrogen in the film during deposition, the amount of defects is reduced. This also gives the material (a-Si:H) a well-defined band gap of 1.75 eV. The material, however, suffers from light-induced metastable defects, known as the Staebler-Wronski effect. This makes the cell less stable over time. This effect is lessened by reducing the thickness of the layer, but this also reduces the amount of light absorption. Under suitable deposition conditions and strong hydrogen dilution, nano- and microcrystallites are formed in the material. These crystallites have a lower defect density and are more resistant against light degradation compared to a-Si. It also shows increased absorption in the red and infrared spectrum [3].

a-Si cells are mostly used in multi-junction devices, together with nanocrystalline silicon and alloy materials. By alloying with germanium, for example, the band gap decreases, absorbing lower energy photons. The highest efficiency cell for a single junction a-Si device is 10.1%, while the record efficiency for a multi-junction device is 12.3% [11]

2.5.2 Cadmium Telluride (CdTe)

CdTe is an ideal absorber because of the direct band gap of 1.5 eV and an absorption coefficient of about 10^5 cm^{-1} in the visible region, which means that a layer thickness of only a few micrometres is needed to absorb most of the photons. CdTe can be made using a variety of deposition methods: devices with efficiencies over 10% have been made using several techniques. Despite these properties, the top efficiency has only gone from 15.8% to 16.7% [11] over the past decade, due to a lack of research. Another issue which needs to be resolved is the toxicity of cadmium: certain European nations ban devices with high cadmium content [3].

2.5.3 CIS, CISE and CIGS(e)

Copper indium sulfide (CuInS_2) has a band gap of 1.53 eV, which is ideal for an application in a solar cell. But the difficulties in controlling the sulfur during the deposition and the diffusion of metals, even at low temperatures, have slowed down the development of this material. But it is possible to replace the sulfur with selenium. Copper indium selenide (CuInSe_2 , or CIS) is a leading candidate for solar cells, with an absorption coefficient of 3 to $6 * 10^5 \text{ cm}^{-1}$ and a band gap of 1 eV [3].

A superior device performance is achieved when the junction is matched to the solar spectrum by increasing the band gap. Alloying with gallium, aluminium or sulfur increases the band gap, which makes it more suitable for high-efficiency single-junction and multi-junction devices [3]. A record 20.3% efficiency has been reached by CIGS [11], but there are certain downsides to this material, which have been mentioned earlier in this report (see Section 2.2). Besides achieving higher efficiencies, research on this type of absorbers has also been focusing on finding new and cost-effective deposition methods, like electrodeposition and electrospraying [3, 28, 29].

2.5.4 III-V materials

Direct band gap III-V semiconductors, such as gallium arsenide (GaAs) and indium phosphide (InP) are also promising materials for solar cells. They have a higher efficiency in comparison to silicon cells. A record efficiency of 28.3% [11] for a thin film single-junction cell of GaAs has been measured. The III-V materials are usually used in multi-junction cells, having achieved a 43.5% efficiency in a GaInP/GaAs/GaInAs setup and a 41.6% efficiency by using a GaInP/GaInAs/Ge multi-junction cell [11].

III-V solar cells are used a lot in space applications because of their higher efficiency than silicon and the fact that III-V materials are more resistant to high energy radiation [30]. The downside is that these type of solar cells are too expensive for large-scale commercial applications [3].

2.5.5 Dye-sensitized solar cells

Dye-sensitized solar cells (DSSCs) are unique to other solar cells because electron transport, light absorption and hole transport are all handled by different materials in the cell. The dye, which acts as the absorber material, is anchored to a wide band gap semiconductor, such as titanium oxide, tin oxide or zinc oxide. When the dye absorbs light, the excited electron rapidly transfers to the conduction band of the semiconductor, which carries the electron to one of the electrodes. A redox couple (using an electrolyte) then reduces the oxidized dye back to its neutral state and transports the positive charge to the counter-electrode. The most employed DSSCs use a ruthenium-based dye and an iodide/triiodide redox couple. Recent research into organic dyes with a lower band gap using a cobalt reduction couple has led to a efficiency of 12.3% [31].

There has been a relatively slow progress in record values for DSSC efficiency over the last 10 years, which is partially due to the fact that ruthenium-based DSSCs have maximum efficiency of around 13% . The production process of the DSSC is relatively cheap, but the materials itself are quite expensive. Another disadvantage of this type of cells is the liquid electrolyte, which can freeze at low temperatures, or expand at higher temperatures. This makes sealing the cell a problem. Recent research has sought to replace the liquid electrolyte with a solid one [31].

2.5.6 Quantumdot absorber

The quantum dot absorber solar cell can be seen as an alternative to the DSSC. The ability to tune the electronic states of quantum dots (QDs), by varying the size together with the solution based preparation, makes them

very interesting as potential absorbers in a so-called extremely thin absorber solar cell (eta-SC). The tunability of the band gap makes lead sulfide (PbS) and lead selenide (PbSe) QDs (which have a bandgap of 0.41 eV and 0.27 eV respectively) more viable by shifting their bandgap to an optimal value. An advanced device structure consisting of SnO:F/TiO₂/PbS-QD/Au has shown the highest efficiency of 5.1%.

Although a lot of research must still be done on quantum dots because of their low efficiency, the quantum dot absorbers are very promising. Both PbS and PbSe quantum dots have shown multiple exciton generation [32] (i.e. a single photon generates more than one electron-hole pair), which can push these absorbers over the Shockley-Queisser limit [33].

2.5.7 Organic absorbers

Interest in organic solar cells stems primarily from the ease of processing, because devices use polymers as part of their construction. Organic semiconductors generally have poor charge carrier mobility, having a big effect on the efficiency. It has on the other hand a high absorption coefficient (order 10^5 cm^{-1}), which gives a high absorption even in layers with a thickness less than 100 nm. Properties can be changed by varying the length of the molecules or by changing the functional group. This changes for example, the band gap. The cost of an organic absorber is very low and the cells have a high mechanical flexibility.

Organic solar cells have been lacking compared to their inorganic counterparts, having an efficiency of around 3 to 5% [34]. But in the last few years, there are several groups who have been reporting efficiencies of over 8%, the record being 10% [11]. One problem with organic solar cells is that they do not last very long, due to degradation under the influence of UV light from the sun [34, 35].

2.6 Electrodeposition

Several methods have thus far been employed to grow a CZTS thin layer: pulsed laser deposition, sputtering, evaporation, sol-gel processing, photochemical deposition, spray pyrolysis and solution based methods. Table 2.1 shows the various CZTS growth methods and the current maximum efficiency achieved by those methods.

Some of these methods, like pulsed laser deposition or sputtering, require a vacuum system, which entails high costs and complex deposition setups. Besides that, a vacuum system is energy consuming, so that the time before the solar cell actually 'generates' energy (i.e., the time after which a solar

Table 2.1: Various growth methods for CZTS and their maximum achieved efficiency

Growth method	Efficiency (%)
Pulsed Laser Deposition	3.14 [36]
Hydrazine-based Solution	10.1 [24]
Sol-gel Sulfurization	2.23 [37]
Evaporation	8.4 [7]
Sputtering	6.7 [26]
Electrodeposition	7.3 [38]

cell has won back the energy needed to produce it) is extended. Another downside is the difficulty from going to small to large scale application. Although many methods work fine on a laboratory scale, scaling them up to industrial standards is sometimes not feasible. The benefit of these vacuum-based methods is that it is easier to control what is being deposited, making it easier to get a good stoichiometry. This gives the possibility to apply, for example, a band gap grading in the absorber layer.

Electrodeposition on the other hand is a method which is low cost, environmentally friendly, easy to use and works at room temperature. Besides that, it scales well from a small deposition area in a laboratory to large area deposition required for commercial mass production [7].

Electrochemical deposition of metals and alloys involves the reduction of metal ions from aqueous, organic or fused-salt electrolytes. The reduction of these metallic ions is represented by the following reaction:



where the M represents the metallic compound and z the charge. The most basic setup for an electrodeposition experiment would be a beaker with 3 electrodes and the electrolyte (see Figure 2.8). The reference electrode sits at a potential of 0 volt (V), while the cathode, or working electrode, has a negative potential (since metal ions have a positive charge).

The working electrode is where the reduction of ions will take place. The positively charged ions are attracted by the negatively charged working electrode. When they reach the electrode, the reduction reaction (Reaction 2.1) will take place, de-ionizing the atom and forming a solid film. If a conducting substrate is attached to the working electrode, the substrate will also be a location for reduction reactions (since it will have the same potential as the electrode). This enables the deposition of thin films on substrates using electrodeposition. The electrons are either supplied by an external power source or by the electrolyte itself (electroless deposition) [40].

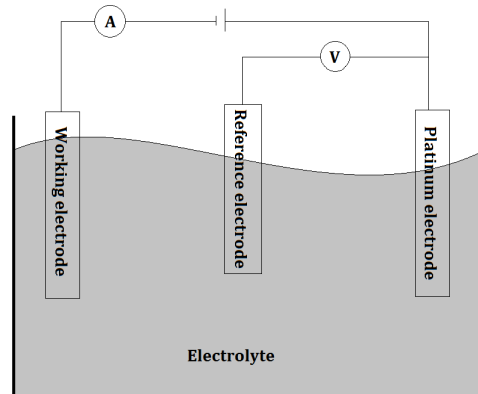


Figure 2.8: Basic electrodeposition setup with three electrodes. Adapted from [39].

Different chemical species have different affinities for reduction, called the reduction potential. This affinity is measured in volt. A species with a lower reduction potential will give off its electrons to a species with a higher reduction potential. The value of the reduction potential of a species is relative to the Standard Hydrogen Electrode (SHE), which is set at 0 V [40]. In practice, reference electrodes are made of other materials, such as silver chloride or calomel (mercury(I) chloride). These electrodes have a potential with respect to SHE, which needs to be taken into account when making measurements or gathering data. The conversion can be made as follows:

$$E_{WE} = E_{SHE} - E_{12} \quad (2.2)$$

where E_{SHE} is the reduction potential with respect to the SHE, E_{WE} the measured reduction potential at the working electrode (the electrode in the experiment) and E_{12} the potential of the reference electrode with respect to the SHE [40]. To make deposition on the working electrode (and an attached substrate) happen, the potential of the electrode must be lower than the reduction potentials of the materials that are to be deposited.

There are two ways of doing a deposition for a multicomponent layer: a single step electrodeposition, where all the compounds are contained in the same solution, or a sequential deposition, where different layers are deposited in a sequence. While the latter will require annealing to mix the different layers and form the desired crystal structure, it is possible for single step electrodeposition to form the crystal structure immediately [41–43]. As-deposited films that need annealing are also known as precursors.

3. Experimental details

The goal is to find the right conditions under which a stoichiometric film of CZTS forms on a substrate. The formation process is divided into two steps: electrodeposition and annealing. Electrodeposition was done in two ways. In the first experiments, the electrolyte contained all four constituents of CZTS (electrolyte 1). Although small amounts of CZTS can form during electrodeposition, secondary phases such as copper sulfide and tin sulfide will make up the bulk of the deposited film. To turn these secondary phases into CZTS proper, an annealing step can be done after deposition.

In a later experiment, deposition with only copper, zinc and tin was attempted (electrolyte 2). This film must be annealed in a sulfur environment to incorporate the sulfur and create the CZTS film.

The influence of sulfur in the precursors seems debatable in the literature. Platzer-Björkman et al. [44] reported larger grains when no precursor sulfur was available, while Katagiri et al. [45] reported a dramatic increase in grain size when they did use sulfur. It is however pointed out that introduction of sulfur in the precursor leads to a more dense and uniform film [44]. For this reason, both methods were used in this project.

Unless otherwise mentioned, all parameters and procedures hold for both electrolytes. A list of equipment used during the experiments can be found in Appendix B. A full explanation of the electrodeposition experiment can be found in Appendix C.

3.1 Substrate

In electrodeposition, the substrate must be conducting in order to grow films. In this experiment, the substrate consisted of silicate glass coated with a thin film of ITO (indium tin oxide), between 150 and 200 nm thick and a deposition area of about $1 \times 2 \text{ cm}^2$. Before starting the deposition, the substrate was cleaned in an ultrasonic bath using detergent, acetone, ethanol and deionized water. After the cleaning the substrates were dry-blown using nitrogen.

3.2 Deposition parameters

The electrodeposition experiment makes it possible to vary a lot of different parameters: applied voltage, concentrations of materials, temperature, pH value and deposition time. Each parameter and its possible influence on the growing film will be explained shortly. During our experiments, we varied the applied voltage and deposition time, while temperature, pH-value and concentrations were kept constant.

3.2.1 Applied voltage

The applied voltage has two functions. First of all, a certain voltage is needed before reduction of metal ions at the working electrode can take place (see Section 2.6). The second function is that the potential influences the deposition rate of the ions. The limiting factor of deposition rate is either the rate at which ions arrive at the surface of the electrode or the rate at which electrons are transferred from the electrode to the depositing ion. The rate of electron transfer is related to the electrical overpotential (the difference between applied potential and reduction potential) applied to the working electrode, which is connected to the substrate. A higher potential will speed up growth, but a voltage which is too high leads to bad adsorption to the surface [40, 46].

For electrolyte 1, earlier research suggests potentials around -1.05 V [42, 43, 47]. For electrolyte 2, research indicates a potential of -1.15 V [48].

3.2.2 pH value

Keeping the electrolyte slightly acidic (between a pH-value of 4.5 and 5) restricts the mobility and precipitation of H^+ ions in the solution [42]. This is done with 0.1 mole per liter (M) tartaric acid, or 2,3-dihydroxybutanedioic acid ($C_4H_6O_6$), as suggested by earlier research [42].

3.2.3 Concentration of materials

In electrodeposition, the influence of the concentration of materials in the electrolyte is clear: higher concentration will generally lead to larger amounts deposited. For CZTS, one option is to have the four components stoichiometrically available in the electrolyte (i.e., copper:zinc:tin:sulfur is 2:1:1:4). However, various factors influence the deposition rate of different elements. Therefore, the concentrations used in electrolyte 1 are as follows: 0.02 M copper sulfate, 0.02 M tin sulfate, 0.01 M zinc sulfate and 0.02 M sodium

thiosulfate. The same concentrations were used in electrolyte 2, with the omission of the sodium thiosulfate. The value of tin is higher, as tin tends to evaporate from the film during annealing due to its low melting temperature (231°C). These values are based on earlier research [42, 43].

3.2.4 Time

The deposition time determines the amount of material deposited on the substrate. Depositing for too long, however, leads to powder formation on top of the layer, without new layers being formed. On the other hand, if the deposition time is not long enough, then the film will be too thin, and may disappear completely after any annealing. Earlier research suggests growth times should be around 40-45 minutes [42, 43, 47].

3.2.5 Temperature

Although higher temperatures increase deposition rates [40], this could have detrimental effects on our water-based solution. Furthermore, results of other research indicate that growth at room temperature is feasible [18, 42, 43, 46, 47]. Therefore, all depositions were done at room temperature. This is also in line with the philosophy of keeping production cheap and simple.

3.2.6 Complexing agent

The different metals in the electrolyte have different reduction potentials. This could lead to uneven deposition, causing deviations from stoichiometry. A complexing agent is added to bring the reduction potentials of the different metals closer together. In this experiment, trisodium citrate ($\text{Na}_3\text{C}_6\text{H}_5\text{O}_7$) at a concentration of 0.1 M is used (based on earlier research [42, 43]).

3.3 Deposition

The ITO side of the substrate was connected to the working electrode, made of platinum. Using a potentiostat in chronoamperometry mode, a potential was applied over the working electrode, referenced to a silver/silver chloride (Ag/AgCl) reference electrode (which has an electrode potential of +200 mV versus SHE). The sign of the potential of the working electrode needs to be negative, to attract the positive metal ions (which in turn will attract the negative sulfur ions). To determine the optimal growing potential, voltages between -0.75 and -1.20 V were used. Growth times were varied between 20

and 60 minutes. After the deposition, the sample was rinsed with water and dry-blown using nitrogen.

3.4 Measuring film properties

To determine if the film has the desired properties, various measuring techniques were used. An explanation of these techniques can be found in Appendix A. The crystallinity was measured using X-ray diffraction (XRD). This would show if the film formed in the required kesterite crystal structure. The surface morphology and film thickness were determined using scanning electron microscopy (SEM). For thin film solar cells, the layer thickness of CZTS should be around 1 μm . The content of the sample was checked using energy dispersive X-ray spectroscopy (EDX), to see if the film was stoichiometric. To determine the energy band gap of the film, optical absorption spectroscopy was used.

3.5 Annealing

As explained earlier, during deposition from electrolyte 1, an amorphous film is grown, consisting of copper sulfide, zinc sulfide, tin sulfide and other mixing phases. For electrolyte 2, only the three metals will be present on the film. An annealing treatment is needed in both cases, to form the actual CZTS and to form a stronger bonding with the substrate. The chemical reactions forming CZTS during annealing are shown here [12]:



Even though sulfides are already present in the film (in case of electrolyte 1), some copper, zinc and tin has not bonded with sulfur yet. To allow enough time for this during the annealing process, the temperature was raised at a small rate of 3°C/minute. This was done for all annealing processes.

Annealing was done in two different ways. The first was to anneal the sample in a nitrogen rich environment (only for films deposited with electrolyte 1). But EDX measurements showed that the samples had low sulfur content after annealing and XRD measurements showed that no actual crystalline CZTS was formed. So instead of annealing in a nitrogen environment,

we switched to a sulfur rich environment. This was done by adding excess sulfur powder in the annealing chamber (about 1 gram), which leads to sulfur vapor at annealing temperatures. The sulfur vapor then mixes with the film, causing CZTS to form.

3.6 Cyclic Voltammetry

Cyclic voltammetry (CV) is an electroanalytical technique used to study redox systems. It enables the electrode potential to be rapidly scanned in search of redox couples. The measurement starts at a certain potential V_1 (0 V in our experiment) and will go to another potential V_2 (-1.5 V in our experiment) at a constant scan rate (0.1 V/s in our experiment). When it has reached potential V_2 , it will go back to the starting potential V_1 . During this sweeping of the potential, which can be done several times in a row, the current is measured.

For a reversible system, the forward scan might trigger oxidation of the electrolyte, while the reverse scan triggers the opposite reaction (reduction) or the other way around. The graph is expected to look the same in the forward and reverse direction. An example of a cyclic voltammogram can be seen in Figure 3.1. Peaks in the graph indicate at which potentials reduction or oxidation occurs.

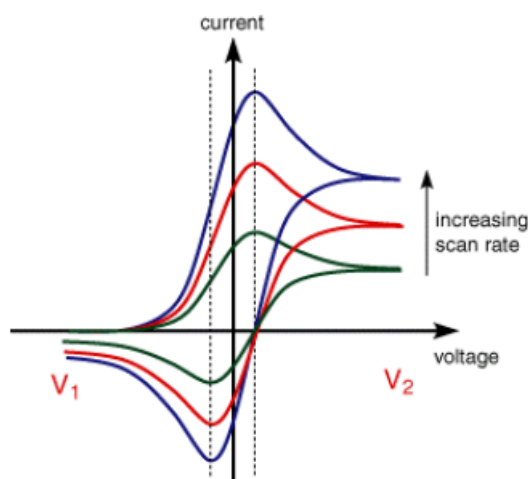


Figure 3.1: Typical voltammogram for a reversible system at different scan rates. The dashed lines indicate where reduction or oxidation takes place. [49]

Electrodeposition is not a reversible system, since material is being deposited on the electrode, changing the electrical properties of both the elec-

trolyte and the electrode. This means that the voltammogram will not be symmetric. But the graph can give a certain indication of the required potential to reduce all the compounds in the electrolyte [49].

4. Results

This chapter will present the results obtained from our experiments. The results will be given in chronological order, explaining choices and conclusions we made during the project.

4.1 What to expect

This section will give a short overview of the results we should expect from measurements in case CZTS is formed. Since CZTS is an absorber, a thick enough film should be opaque to the naked eye (90% absorption for a 500 nm film). This gives a good quick estimation whether a thick film of CZTS has formed or not.

XRD measurements should give something similar to 4.1. The (112)-peak (located at $2\theta=28.4^\circ$) and the (220)-peak (located at $2\theta=47.3^\circ$) are the most prominent peaks in the spectrum.

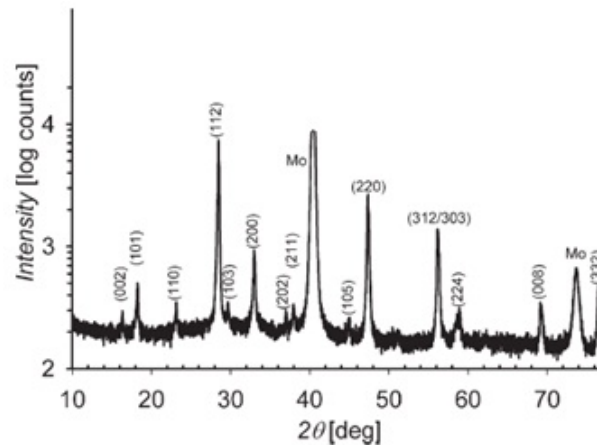


Figure 4.1: Diffractogram of CZTS on a molybdenum substrate. Numbers between brackets are the Miller indices of various planes. Adapted from [50].

The SEM images in Figure 4.2 are taken from the paper of Pawar et al.,

whose experimental parameters we used to start off with. This means our results with electrolyte 1 should be similar to theirs.

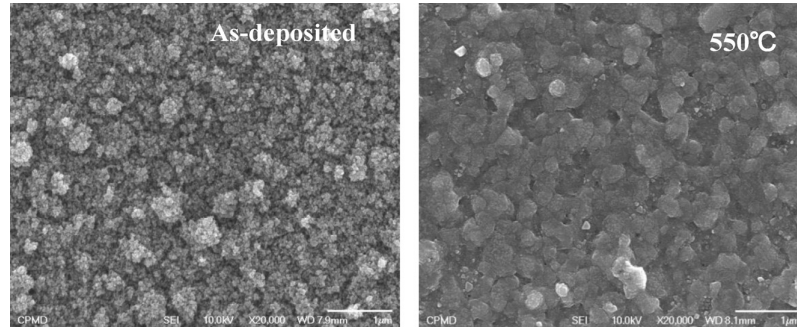


Figure 4.2: SEM images of as-deposited and annealed CZTS. Adapted from [42].

For electrolyte 2, the XRD graph should be like the same as for electrolyte 1, given in 4.1. The as-deposited film, however, will look different. Chen et al. [48] also used an electrolyte which did not contain sulfur. The difference is that they annealed in a selenium environment instead of a sulfur environment. There have been no reports of doing electrodeposition without sulfur, followed by sulfurization step. This makes it unclear what to expect for this method.

4.2 Optimizing potential with electrolyte 1

The first objective was to find a potential or range of potentials which formed a suitable film on the ITO substrate. A good film in this case means a film with good (macroscopic) coverage of the substrate and sticks to the surface well (i.e., does not let go during rinsing). As discussed in Section 3.2.1, earlier research indicates the potential should be around -1.05 V. To verify this, we used potentials from -0.75 to -1.15 V. For potentials higher than -0.95 V, the films would not bond strongly with the substrate, causing it to fall off during rinsing. Potentials of -1.15 V and lower, on the other hand, lead to bad adsorption, again making the film come off during rinsing. This confirms that good films grow between -1.00 and -1.10 V.

4.3 XRD and EDX results

To check the crystallography of films grown at the correct potentials, we performed XRD measurements on two samples (CZTS35, grown at -1.0 V

for 20 minutes, and CZTS36, grown at -1.05 for 25 minutes). The results of these measurements can be seen in Figure 4.3, with an XRD measurement of the substrate as comparison (Figure 4.3.c). The graph shows no peaks corresponding to CZTS, which means no crystalline film was grown. Examining these samples with EDX, however, showed prominent peaks from the substrate, meaning that the film was too thin (see Figure 4.3.d). So the deposition time needed improvement.

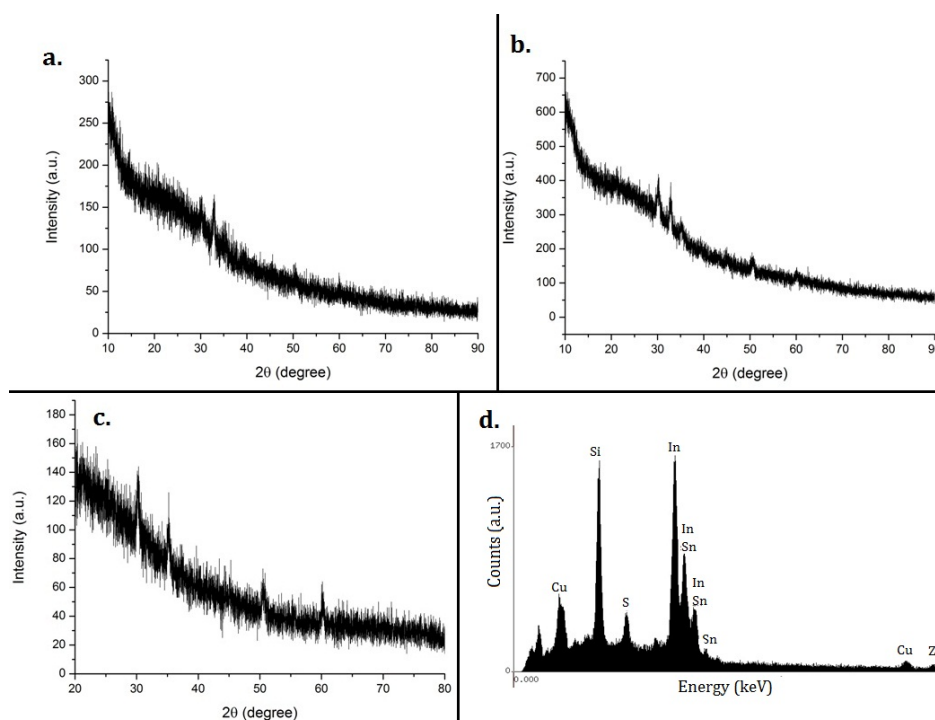


Figure 4.3: XRD measurement of a) CZTS35, b) CZTS36 and c) the substrate (ITO), d) EDX measurement of CZTS35. a) and b) show no peaks other than substrate peaks, which indicates no crystalline film has formed. The EDX measurement shows high indium and silicon peaks, originating from the substrate, which suggest that the film is too thin.

4.4 Deposition time

Next we tried to find the optimal deposition time. Films were grown between 10 and 60 minutes at -1.05 V. Deposition times around 40 to 45 minutes were suggested to be optimal, as discussed in Section 3.2.4. Short deposition times (< 40 minutes) resulted in not enough material being deposited on the

substrate, while films grown for long times (> 50 minutes) had powder formation. These results are again in agreement with earlier research, discussed in Section 3.2.4. Combining the previous results, good films from electrolyte 1 grow at potentials between -1.0 and -1.1 V, and deposition times between 40 and 50 minutes.

4.5 XRD, SEM and EDX measurements

Using SEM, we checked the coverage of the films grown in the previous experiment. SEM images of samples CZTS53 through CZTS56 (deposited at -1.05 for 20, 30, 40 and 50 minutes respectively) are shown in Figure 4.4. The images show that coverage increases with deposition time, which further supports deposition times between 40 and 50 minutes.

XRD measurements on an as-deposited sample (see Figure 4.5) showed that no crystalline film was formed. This, combined with earlier research [41–43, 47, 51], implies that the films need annealing before crystalline CZTS will form.

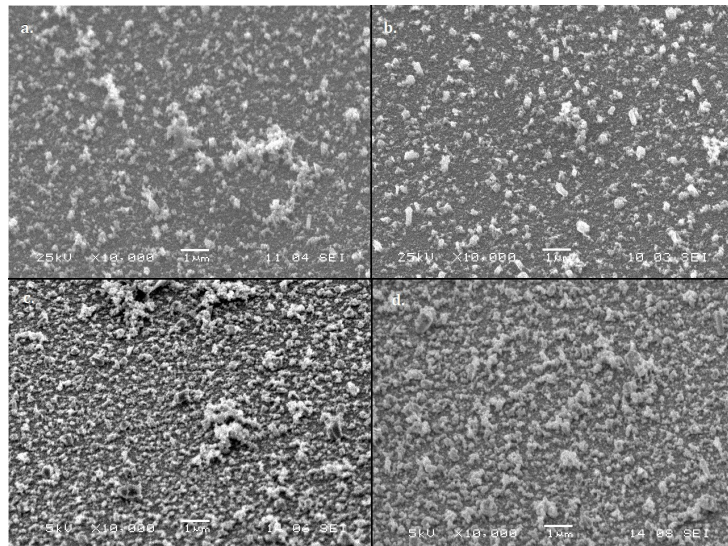


Figure 4.4: SEM images of a) CZTS53, b) CZTS54, c) CZTS55 and d) CZTS56. Images show that coverage increases with deposition time.

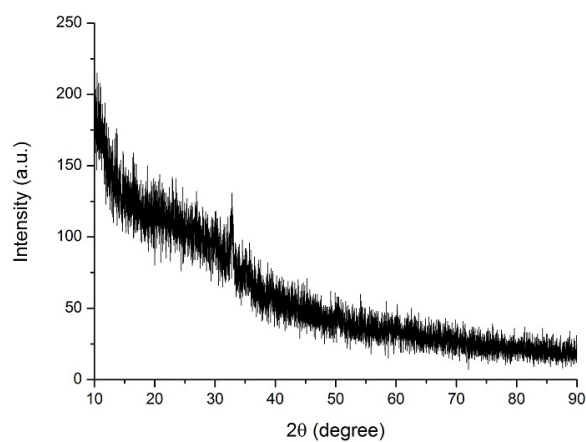


Figure 4.5: XRD measurement of CZTS55. Again no crystalline film has formed.

4.6 Annealing in nitrogen environment

To improve crystallinity, samples CZTS59 (grown at -1.1 V for 40 minutes) and CZTS60 (grown at -1.1 for 50 minutes) were annealed in a nitrogen environment (to suppress any oxidizing reactions). The samples were annealed for 60 minutes at 400°C. After this, XRD measurements were done (see Figure 4.6), which showed no crystalline CZTS.

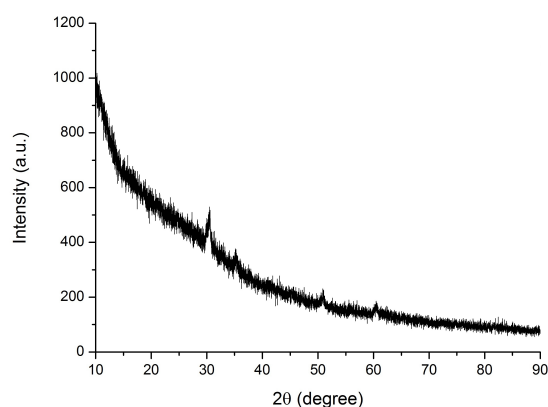


Figure 4.6: XRD measurement of a sample annealed in a nitrogen environment. No crystalline CZTS forms after annealing in a nitrogen environment.

However, EDX measurements also indicated that the four components were not deposited on the film in the correct ratios. The films lacked primar-

ily in sulfur. Because a sulfur ion is negatively charged, it is only deposited on the film due to attraction by local positive charges created by the copper, zinc and tin. This explains the low sulfur count on the films. For this reason the nitrogen environment was replaced by a sulfur environment, to improve the amount of sulfur on the films and create stoichiometric CZTS.

4.7 Annealing in sulphur environment

Samples CZTS65 (grown at -1.1 V for 40 minutes) and CZTS66 (grown at -1.05 V for 40 minutes) were annealed in a sulfur environment for 60 minutes at 500°C. After annealing, the film was mostly transparent. Since CZTS is supposed to be an absorber, this indicates that the film is probably not thick enough. Figure 4.7 shows images of the surface of CZTS66, before and after annealing. The annealing process seems to smoothen the surface, although copper sulfide crystals (measured with EDX) remain visible. XRD measurements, seen in Figure 4.8, show that CZTS peaks appear. However, the peaks are still very small, indicating that either the crystallization process is not fully completed, or that not much CZTS is present. A low-magnification SEM image of the surface (Figure 4.9) shows island formation. Instead of a uniform layer, patches of copper sulfide and CZTS form during annealing. EDX confirms that some islands contain near-stoichiometric CZTS (see Table 4.1).

To see if further annealing improves the film, the two samples (CZTS65 and CZTS66) were annealed at 550°C for 60 minutes, again in a sulfur environment. After annealing, the film was again mostly transparent, indicating that the film is, most likely, still not correct. XRD measurements of CZTS66 (Figure 4.8) show that the crystallinity of the film improves, and SEM images of the surface (see Figure 4.10) show that the film is more uniform when compared to annealing at 500°C (see Figure 4.9). The XRD measurement, however, still shows peaks from the substrate, which means that the film is thin.

Table 4.1: EDX measurement of CZTS island on sample CZTS65, annealed at 500°C.

Element	Presence (%)	Standard deviation (%)	Expected (%)
Copper	26.6	±0.8	25
Zinc	14.5	±0.8	12.5
Tin	11.2	±0.9	12.5
Sulfur	47.7	±0.2	50

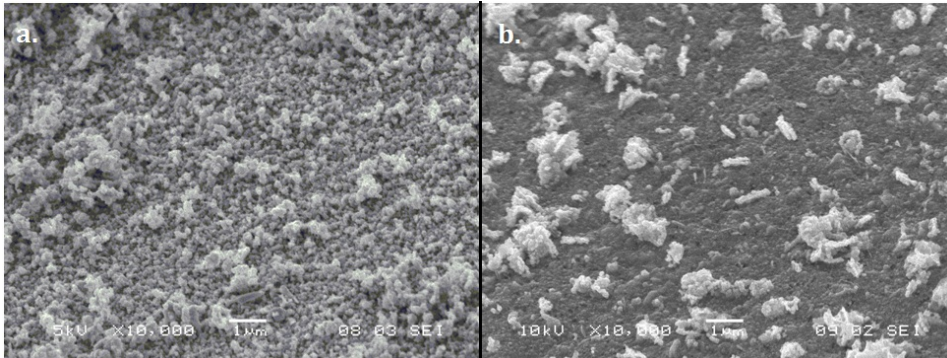


Figure 4.7: SEM images of a) CZTS66 as-deposited and b) annealed at 500°C. Annealing seems to smoothen the surface, but copper sulfide structures remain.

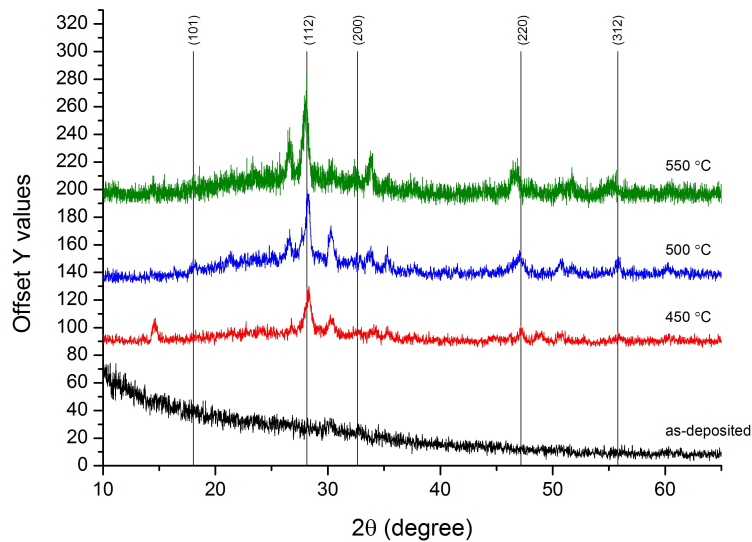


Figure 4.8: XRD measurements of CZTS66 as-deposited and annealed at various temperatures. Annealing improves crystallinity, but substrate peaks remain visible, suggesting the film thickness is too low.

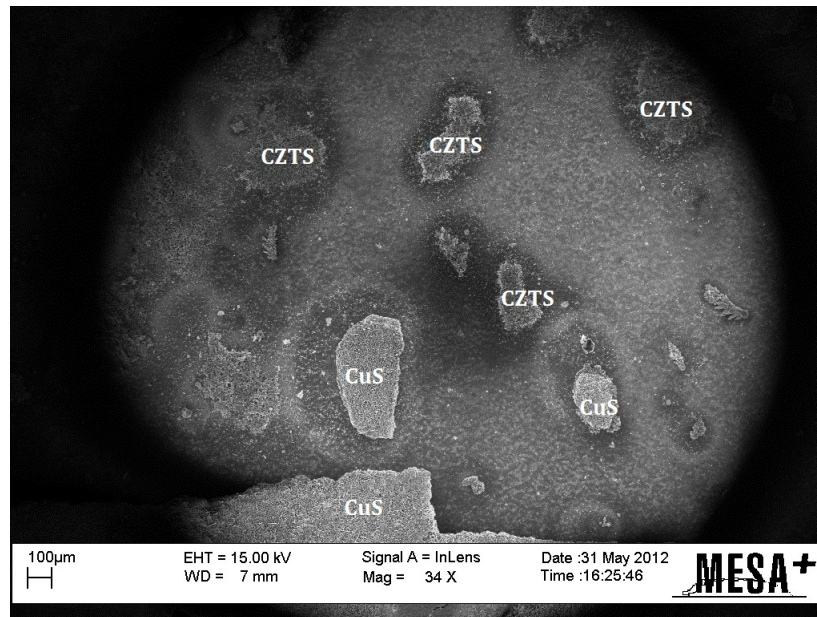


Figure 4.9: Low-magnification SEM image of CZTS66 annealed at 500°C. Islands of CZTS and copper sulfide appear on the surface, instead of a uniform film.

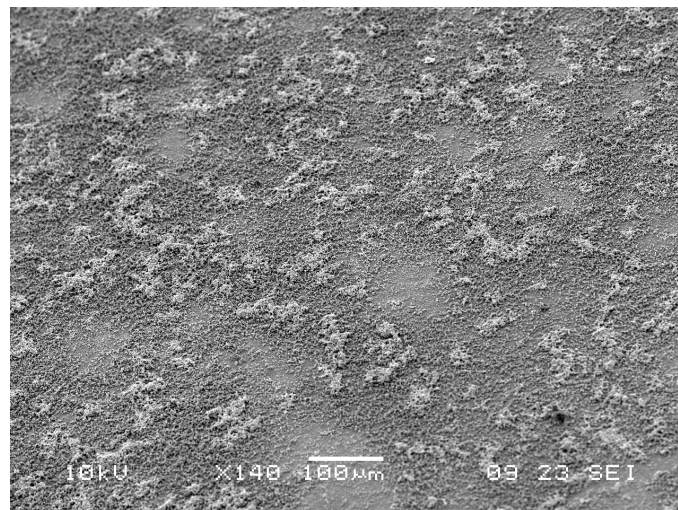


Figure 4.10: Low-magnification SEM image of CZTS66 annealed at 550°C. The film seems more uniform.

4.8 Deposition with electrolyte 2

Since electrolyte 1 did not give satisfying results, another route was tried. A new electrolyte was made containing no sulfur (electrolyte 2); the sulfur was only introduced during the annealing process. Because of the different electrolyte, a different optimal deposition potential was expected. Chen et al. also tried the same route (but annealed in selenium instead of sulfur), using a potential -1.15 V [48]. When applying this voltage in our experiment, however, the film had a bad adhesion, and almost completely fell off during rinsing in water. To still get an indication of which potential to use, a cyclic voltammetry measurement was done. The result of that measurement is shown in Figure 4.11.

There is a very distinct peak around -0.85 V. The reverse peak at around -0.5 V does not represent the reduction of the elements (since the current at that position is positive). Therefore, it is expected that the optimum potential lies around -0.85 . To verify this, depositions were done for 30 minutes, starting with a voltage of -0.80 V and increasing to -1.15 V.

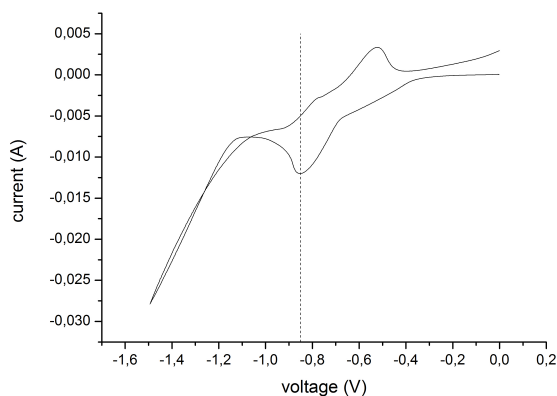


Figure 4.11: Cyclic voltammetry of electrolyte 2. The peak around -0.85 V indicates reduction.

Films deposited at a potential of -1.00 V and lower showed a non-adhesive top layer, which would let go during rinsing. The other films, deposited at a potential between -0.8 V and -0.95 V, had a metallic-looking surface. This surface was uniform on a macroscopic scale. This is already different from films deposited with electrolyte 1, which were not uniform macroscopically. The potential of -1.15 V used by Chen et al. did not work in this experiment, which is probably due to usage of different concentrations of materials.

Two of the good samples (CZTS79 and CZTS80 grown at -0.85 V and -0.90 V respectively) were then annealed in a sulfur environment. The temperature was increased to 450°C and kept there for 30 minutes. This was done so that secondary phases had enough time to form, since no sulfur was in the film before annealing. The sulfur has to diffuse into the entire layer during annealing. After that, the temperature was increased to 500°C and kept at that temperature for 60 minutes. As explained earlier, the higher temperature should make sure that the secondary phases melt together to form CZTS. To see if this result was any different from the experiments with electrolyte 1, characterizations were done using XRD (see Figure 4.12 and SEM (see Figure 4.13).

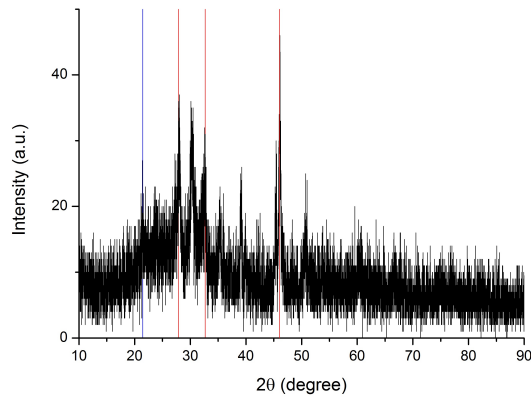


Figure 4.12: XRD of CZTS80 post-annealing. The film is amorphous, but small peaks of SnS (indicated orange) and Sn_2S_3 (indicated blue) show that there is an excess of tin.

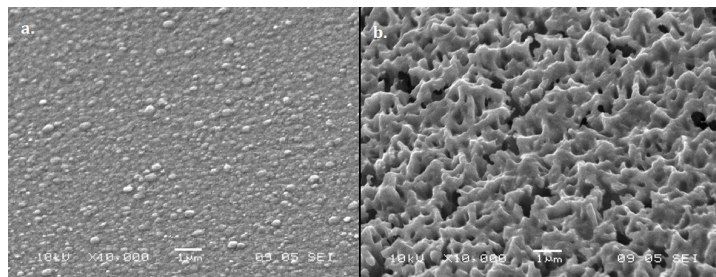


Figure 4.13: SEM images of samples grown in electrolyte 2. a) as-deposited and b) post-annealing. The entire deposition area was uniform.

The post annealing image (4.13.b) looks very different compared to annealed films from electrolyte 1 (see Figure 4.7). Whereas the earlier samples

were not uniform and contained islands of CZTS and secondary phases, these samples were uniform across the entire deposition area. However, the XRD shows that the film is amorphous, and the small peaks that can be seen could belong to tin sulfides. This means that there is too much tin available in the precursor.

5. Discussion

The results of the experiments bring up questions and new problems. Here, possible answers and/or solutions will be discussed.

The most glaring issue is the discrepancies between the research done by Pawar et al. [42] and our experiments with electrolyte 1. Most parameters (concentrations, applied potential, deposition time, annealing temperature and time) were identical, and while they got good formation of CZTS, we did not. One difference between this project and the research done by them is the fact that they annealed in an argon environment, against the sulfur environment we used. This begs the question: Why did they get enough sulfur on the film during deposition, and we did not? The only difference during electrodeposition between the two projects is the substrate choice.

Pawar et al. used both ITO and molybdenum substrates, while we only used ITO substrates. Their paper is not clear on which substrates gave which results, but their XRD measurements were performed on samples with molybdenum substrates. The results of those measurements were promising, but no such measurements were done for ITO substrates. This makes the comparison more difficult, but one possible conclusion is that electrodeposition of CZTS on ITO substrates with all four elements in the electrolyte is not a valid option. To investigate this further, electrodeposition on molybdenum can be done to see if that yields better results.

The island formation (Figure 4.9) is also an interesting point. Although the simple explanation would be that there is not enough material available to cover the surface, there is another option. It might be that CZTS tends to cluster and form islands instead of spreading over the surface equally. This can be investigated by measuring the height of the islands. If the islands are of substantial height, this would indicate clustering behavior, while islands of small height would mean that the island growth is just a result of lack of material. We attempted this with an atomic force microscope (AFM). However, the scale on which an AFM operates is too small for this purpose, so it could not give us a definitive answer. Therefore, another method needs to be used for this.

In case of clustering behavior, the next step is to wonder what is causing

it. Is it intrinsic to CZTS, or does it have to do with the substrate? Solving the island growth issue might be a matter of getting more material on the film. However, since lower voltages and longer growth times are not an option (as explained in Section 4.2 and Section 4.4), this could be harder than it sounds. If the island formation is due to problems with the substrate, then the earlier suggested option of investigating a molybdenum substrate can also be applied here.

The experiments with electrolyte 2 showed promising results. The electrodeposited films were uniform both macroscopically and microscopically. After annealing in sulfur, the SEM images (see Figure 4.13) showed drastic changes in the surface morphology. The XRD measurement (Figure 4.12) showed hints of tin sulfides, but due to the high noise levels, this cannot be said with high certainty. The XRD does indicate that the film is amorphous, since the few visible peaks are very small. EDX measurements can give more insight as to what is present on the samples.

If the tin sulfides are indeed present on the sample, then that would indicate that the as-deposited films (and therefore, the electrolyte) contained too much tin. Future research could change the concentrations of the materials in the electrolyte to acquire better ratios of the three metals on the film.

Using XRD might not be the best tool to measure the correct phase of the film. When looking at the phase diagram, there are a lot of possible secondary phases. Each of these can give a peak in the diffractogram. Most of the secondary phases have peaks which lie very close to the peaks of CZTS, due to similar crystal structure. A few of these similar peaks can be seen in Table 5.1.

Table 5.1: XRD peak locations of CZTS, cubic CTS and cubic ZnS [52].

CZTS		Cubic-CTS		Cubic-ZnS	
2θ (degree)	Plane	2θ (degree)	Plane	2θ (degree)	Plane
28.44	1 1 2	28.45	1 1 1	28.50	1 1 1
32.93	2 0 0	32.96	2 0 0	33.03	2 0 0
33.02	4 0 0	-	-	-	-
47.33	2 0 4	47.31	2 2 0	47.40	2 2 0
56.09	3 1 2	56.13	3 1 1	56.24	3 1 1

This makes it hard to distinguish CZTS or the secondary phases in a diffractogram (although a very broad peak can give an indication). Some of the other secondary phases (Cu_2S and SnS) can be identified due to the peak positions which are entirely different from CZTS. But Table 5.1 shows that this is not the case for all phases. A technique which can give a better indication of the presence of secondary phases and actual CZTS is Raman

scattering [52, 53] because each material has a peak position which is more distinct than in XRD.

Instead of annealing in a elemental sulfur environment, some research groups anneal in a hydrogen sulfide (H_2S). Films created in this way also yielded good results, although no straight comparison between the two methods have been made. Investigating annealing in H_2S and comparing it with annealing in elemental sulfur could be a basis for future experiments. An important thing to note, though, is that H_2S is highly flammable and toxic, and must therefore be handled with care [5].

6. Conclusions

Our goal was to find out if electrodeposition, combined with annealing, was a good method of growing CZTS thin films on ITO substrates. We used two different electrolytes (one including and one without sulfur), to study the influence of sulfur during deposition.

The experiments with sulfur included yielded films with good adhesion and thickness for potentials between -1.0 and -1.1 V and deposition times between 40 and 50 minutes. However, no samples had full substrate coverage of CZTS after annealing in both nitrogen and sulfur. The CZTS formed in islands, instead of spreading evenly over the surface. This is possibly due to the choice of substrate.

The films grown without any sulfur in the electrolyte showed more promising results, creating uniform films when grown at potentials between -0.8 and -0.95 V. The surface morphology changed drastically after annealing in sulfur. Although the composition of the electrolyte needed improvement, since too much tin was present on the films, this might be the better procedure to grow stoichiometric CZTS films.

Bibliography

- [1] O. Morton, *A new day dawning? Silicon Valley sunrise*, Nature, Vol. **443**, p. 19-22, **2006**.
- [2] G. Adiboina, *Thin film photovoltaic (PV) cells market analysis to 2020*, The Alternative Energy eMagazine (published online), **2010**.
- [3] K.L. Chopra, P.D. Paulson and V. Dutta, *Thin-film solar cells: An overview*, Progress in Photovoltaics Research and Applications, Vol. **12**, p. 69-92, **2004**.
- [4] J. Emsley, *Nature's building blocks: An A-Z guide to the elements*, 1st edition, Oxford University Press, **2002**, .
- [5] ScienceLab, *Material Safety Data Sheets*
www.sciencelab.com/msdsList.php, Retrieved: **15-05-2012**.
- [6] P.K. Sarswat and M.L. Free, *A study of energy band gap versus temperature for Cu_2ZnSnS_4 thin films*, Physica B, Vol. **407**, p. 108-111, **2011**.
- [7] B. Shin, O. Gunawan et al., *Thin film solar cell with 8.4% power conversion efficiency using an earth-abundant Cu_2ZnSnS_4 absorber*, Progress in Photovoltaics: Research and Applications (published online), **2011**.
- [8] M. Ohring, *Materials Science of Thin Films*, 2nd edition, Elsevier Inc., **2002**, .
- [9] I.M. Dharmadasa, A.P. Samantilleke et al., *New ways of developing glass/conducting glass/CdS/CdTe/metal thin-film solar cells based on a new model*, Semiconductor Science and Technology, Vol. **17**, p. 1238-1248, **2002**.
- [10] W. Shockley and H.J. Queisser, *Detailed balance limit of efficiency of p-n junction solar cells*, Journal of Applied Physics, Vol. **32**, p. 510-519, **1961**.

-
- [11] M.A. Green, K. Emery et al., *Solar cell efficiency tables (Version 39)*, Progress in Photovoltaics: Research and Applications, Vol. **20**, p. 12-20, **2011**.
- [12] H. Flammersberger, *Experimental study of Cu_2ZnSnS_4 thin films for solar cells*, Uppsala Universitet, **2010**.
- [13] G.F. Bernardini, D. Borrini et al., *EPR and SQUID magnetometry study of Cu_2FeSnS_4 (stannite) and Cu_2ZnSnS_4 (kesterite)*, Phys. Chem. Minerals, Vol. **27**, p. 453-461, **2000**.
- [14] S.R. Hall, J.T. Szymanski and J.M. Stewart, *Kesterite, $Cu_2(Zn,Fe)SnS_4$ and Stannite $Cu_2(Fe,Zn)SnS_4$, structurally similar but distinct minerals*, Canadian Mineralogist, Vol. **16**, p. 131-137, **1978**.
- [15] J.P. Leitão, N.M. Santos et al., *Study of optical and structural properties of Cu_2ZnSnS_4 thin films*, Thin Solid Films, Vol. **519**, p. 7390-7393, **2010**.
- [16] K. Ito and T. Nakazawa, *Electrical and optical properties of stannite-type quaternary semiconductor thin films*, Japanese Journal of Applied Physics, Vol. **27**, p. 2094-2097, **1988**.
- [17] S. Chen, J.H. Yang et al., *Intrinsic point defects and complexes in the quaternary kesterite semiconductor Cu_2ZnSnS_4* , Physical Review B, Vol. **81**, p. 245204 (10 pages), **2010**.
- [18] J.J. Scragg, *Studies of Cu_2ZnSnS_4 films prepared by sulfurisation of electrodeposited precursors*, University of Bath, **2010**.
- [19] T. Shibata, Y. Muranushi et al., *Photoconductive properties of single-crystal $2H-SnS_2$* , Journal of Physics and Chemistry of Solids, Vol. **51**, p. 1297-1300, **1990**.
- [20] W. Ahmed M.Y. Nadeem, *Optical properties of ZnS thin films*, Turkish Journal of Physics, Vol. **24**, p. 651-659, **2000**.
- [21] C. Wu, Z. Hu et al., *Hexagonal Cu_2SnS_3 with metallic character: Another category of conducting sulfides*, Applied Physics Letters, Vol. **91**, p. 143104 (3 pages), **2007**.
- [22] H. Wang, *Progress in thin film solar cells based on Cu_2ZnSnS_4* , International Journal of Photoenergy, Vol. **2011**, p. 801292 (10 pages), **2011**.

- [23] U. Wang, *The promise and unanswered questions about CZTS solar technology*
www.renewableenergyworld.com/rea/news/article/2012/06/the-promise-and-unanswered-questions-about-czts-technology, Retrieved: **20-06-2012**.
- [24] D.A.R. Barkhouse, O. Gunawan et al., *Device characteristics of a 10.1% hydrazine-processed $Cu_2ZnSn(Se,S)_4$ solar cell*, Progress in Photovoltaics: Research and Applications, Vol. **20**, p. 6-11, **2011**.
- [25] T. Todorov, O. Gunawan et al., *Progress towards marketable earth-abundant chalcogenide solar cells*, Thin Solid Films, Vol. **519**, p. 73787381, **2011**.
- [26] H. Katagiri, K. Jimbo et al., *Development of CZTS-based thin film solar cells*, Thin Solid Films, Vol. **517**, p. 2455-2460, **2008**.
- [27] K. Oishi, G. Saito et al., *Growth of Cu_2ZnSnS_4 thin films on Si (100) substrates by multisource evaporation*, Thin Solid Films, Vol. **517**, p. 1449 - 1452, **2008**.
- [28] S. Saji, I. Choi and C-W. Lee, *Progress in electrodeposited absorber layer for $CuIn_{1-x}Ga_xSe_2$ (CIGS) solar cells*, Solar Energy, Vol. **85**, p. 2666-2678, **2011**.
- [29] N.M. Muhammad, S. Sundharam et al., *CIS layer deposition through electro spray process for solar cell fabrication*, Current Applied Physics, Vol. **11**, p. S68S75, **2010**.
- [30] T.V. Torchynska and G.P. Polupan, *III-V material solar cells for space application*, Quantum Electronics and Optoelectronics, Vol. **5**, p. 63-70, **2002**.
- [31] B.E. Hardin, H.J. Snaith and M.D. McGehee, *The renaissance of dye-sensitized solar cells*, Nature Photonics, Vol. **6**, p. 162-169, **2012**.
- [32] R.D. Schaller and V.I. Klimov, *High efficiency carrier multiplication in PbSe nanocrystals: Implications for solar energy conversion*, Physical Review Letters, Vol. **92**, p. 186601 (4 pages), **2004**.
- [33] T. Dittrich, A. Belaidi and A. Ennaoui, *Concepts of inorganic solid-state nanostructured solar cells*, Solar Energy Materials and Solar Cells, Vol. **95**, p. 1527-5136, **2010**.

- [34] H. Hoppe and N.S. Sariciftci, *Organic solar cells: An overview*, Journal of Material Science, Vol. **19**, p. 1924-1945, **2004**.
- [35] T.L. Benanti and D. Venkataraman, *Organic solar cells: An overview focusing on active layer morphology*, Phtosynthesis Research, Vol. **87**, p. 73-81, **2005**.
- [36] A.V. Moholkar, S.S. Shinde et al., *Synthesis and characterization of Cu_2ZnSnS_4 thin films grown by PLD: Solar cells*, Journal of Alloys and Compounds, Vol. **509**, p. 7439-7446, **2011**.
- [37] K. Maeda, K. Tanaka et al., *Influence of H_2S concentration on the properties of Cu_2ZnSnS_4 thin films and solar cells prepared by sol-gel sulfuration*, Solar Energy Materials and Solar Cells, Vol. **95**, p. 2855-2860, **2010**.
- [38] S. Ahmed, K.B. Reuter et al., *A high efficiency electrodeposited Cu_2ZnSnS_4 solar cell*, Advanced Energy Materials, Vol. **2**, p. 253-259, **2011**.
- [39] D. Bera, S.C. Kuiry and S. Seal, *Synthesis of nanostructured materials using template-assisted electrodeposition*, Journal of the Minerals, Metals and Materials Society, Vol. **56**, p. 49-53, **2004**.
- [40] M. Paunovic and M. Schlesinger, *Fundamentals of electrochemical deposition*, 1st edition, John Wiley & Sons Inc., **1998**, .
- [41] J.J. Scragg, P.J. Dale and L.M. Peter, *Synthesis and characterization of Cu_2ZnSnS_4 absorber layers by an electrodeposition-annealing route*, Thin Solid Films, Vol. **517**, p. 2481-2484, **2008**.
- [42] S.M. Pawar, B.S. Pawar et al., *Single step electrosynthesis of Cu_2ZnSnS_4 (CZTS) thin films for solar cell application*, Electrochimica Acta, Vol. **55**, p. 4057-4061, **2009**.
- [43] M. Jeon, Y. Tanaka et al., *Formation and characterization of single-step electrodeposited Cu_2ZnSnS_4 thin films: Effect of complexing agent volume*, Energy Procedia, Vol. **10**, p. 255-260, **2011**.
- [44] C. Platzer-Björkman, J. Scragg et al., *Influence of precursor sulfur content on film formation and compositional changes in Cu_2ZnSnS_4 films and solar cells*, Solar Energy Materials and Solar Cells, Vol. **98**, p. 110-117, **2011**.

- [45] H. Katagiri, N. Ishigaki et al., *Characterization of Cu_2ZnSnS_4 thin films prepared by vapor phase sulfurization*, Japanese Journal of Applied Physics, Vol. **40**, p. 500-504, **2000**.
- [46] M. Kurihara, D. Berg et al., *Kesterite absorber layer uniformity from electrodeposited pre-cursors*, Physica Status Solidi, Vol. **6**, p. 1241-1244, **2008**.
- [47] M. Jeon, T. Shimizu and S. Shingubara, *Cu_2ZnSnS_4 thin films and nanowires prepared by different single-step electrodeposition method in quaternary electrolyte*, Materials Letters, Vol. **65**, p. 2364-2367, **2011**.
- [48] Z. Chen, L. Han et al., *$Cu_2ZnSnSe_4$ thin films prepared by selenization of co-electroplated $CuZnSn$ precursors*, Applied Surface Science, Vol. **257**, p. 8490-8492, **2011**.
- [49] D. Andrienko, *Cyclic Voltammetry*
www.mpip-mainz.mpg.de/~andrienk/journal_club/cyclic_voltammetry.pdf, Retrieved: **13-06-2012**.
- [50] T.K. Todorov, K.B. Reuter and D.B. Mitzi, *High-efficiency solar cell with earth-abundant liquid-processed absorber*, Advanced Energy Materials, Vol. **22**, p. 156-159, **2010**.
- [51] C.P. Chan, H. Lam and C. Surya, *Preparation of Cu_2ZnSnS_4 films by electrodeposition using ionic liquids*, Solar Energy Materials and Solar Cells, Vol. **94**, p. 207-211, **2008**.
- [52] P.A. Fernandes, P.M.P. Salomé and A.F. Cunha, *Study of polycrystalline Cu_2ZnSnS_4 films by Raman scattering*, Journal of Alloys and Compounds, Vol. **509**, p. 7600-7606, **2011**.
- [53] P.A. Fernandes, P.M.P. Salomé and A.F. Cunha, *Growth and Raman scattering characterization of Cu_2ZnSnS_4 thin films*, Thin Solid Films, Vol. **517**, p. 2519-2523, **2008**.

A. Measuring Techniques

During the experiments we used several different measuring techniques to retrieve the information needed from the various samples. Properties of interest were energy band gap, film thickness, stoichiometry and surface morphology. The techniques used to determine these characteristics will be explained here.

A.1 X-ray diffraction

X-ray diffraction (XRD) is a technique based on Bragg's law, a geometric law which allows crystallographic properties of the film to be retrieved. Bragg's law can be deduced from the geometry of figure A.1, and is given in the following formula:

$$n\lambda = 2d\sin(\theta) \quad (\text{A.1})$$

where n is an integer, λ is the wavelength of the incoming X-rays, d is the distance between crystal planes, and θ the angle of incidence of the X-rays.

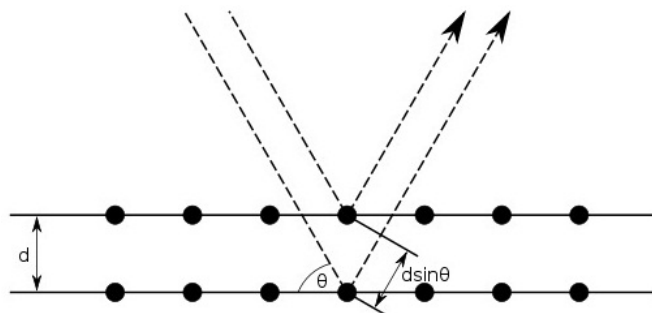


Figure A.1: Geometry of Bragg diffraction. The dashed lines indicate the diffracting X-ray beams, incident at an angle θ . The solid lines indicate crystal planes, separated by a distance d . For constructive interference to occur between the two beams, the extra path length $2d\sin(\theta)$ must be an integer number of wavelengths. [1]

XRD is a technique which uses an X-ray source with fixed λ , and scans over a range of θ . From this, using Bragg's law, d can be calculated. Using crystallographic data, the crystal structure can then be determined. Figure A.2 shows a typical XRD setup.

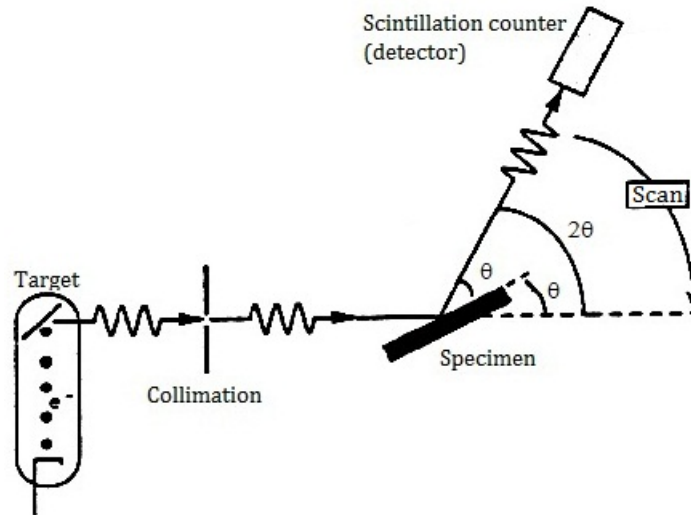


Figure A.2: XRD setup showing the different components. Adapted from [2]

To produce X-rays, a tungsten filament is heated, which makes it give off electrons. These electrons are accelerated in an electric field and collide with a target material (usually copper). If the electron has enough energy, the collision will remove an electron from one of the shells of the material's atoms. The hole created in this way can then be filled by an electron from an outer shell, which leads to photon emission (see Figure A.3). These photons have energies in the X-ray spectrum. The name of these X-rays depends on the shell the electron is removed from and the shell of the electron which fills the void. For example, a $K\alpha$ X-ray means the X-ray is created by an electron moving from the L to the K shell.

The X-rays are collimated and directed towards the sample, and diffracted at various angles θ . A detector scans over a range of angles and counts the incoming photons. The angles where constructive interference occurs will yield larger amounts of photons. Figure 4.1 shows a diffractogram of a CZTS sample grown on a molybdenum substrate. Typical diffractograms will have 2θ on the horizontal axis instead of θ , since 2θ is the angle between the incoming and diffracted beam. The numbers between brackets denote the Miller indices of the various crystal planes.

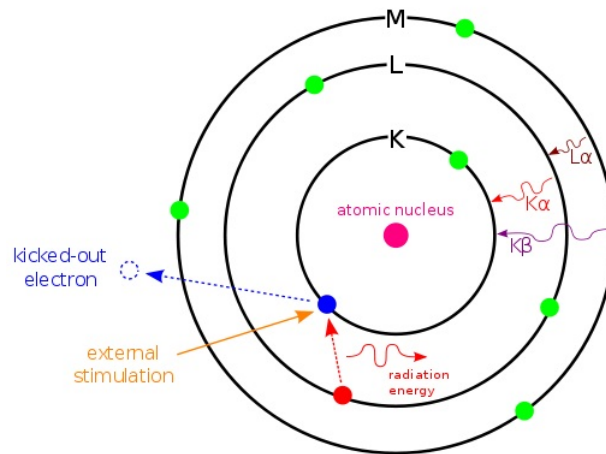


Figure A.3: Emission of X-rays by external stimulation. [3]

A.2 Scanning electron microscopy

Scanning electron microscopy (SEM) is a method to determine surface morphology of a sample. Additionally, some SEM setups have an X-ray detector to perform EDX measurements (see Section A.3). A standard SEM setup is shown in figure A.4.

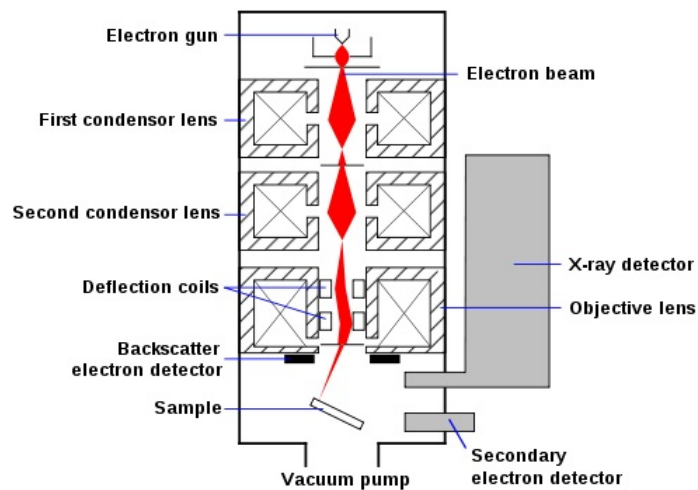


Figure A.4: Typical SEM setup. [4]

The electron gun is the source of primary electrons. Standard electron guns produce electron beams in one of two ways. The first is by heating a tungsten filament to thermionically excite electrons. The second method,

named field emission, is to use an electric field to cause emission of electrons.

The electron beam is focused by one or two condenser lenses. Unlike lenses in normal optic microscopes, these lenses are magnets, which use electromagnetic forces to control the electron beam. The beam then passes through the objective lens, which contains deflection coils. These coils move the beam to scan across the sample.

When the primary electrons collide with the sample, several interactions take place in a so called interaction volume, shown in Figure A.5. Some electrons are reflected by elastic collisions, named backscattered electrons. Inelastic collisions can cause emission of secondary electrons or emission of X-rays. Usually the secondary electrons are used to create SEM images. The amount of secondary electrons depends on the angle of the primary electron beam with the surface of the sample, where smaller angles lead to higher secondary electron yield (see Figure A.5.b).

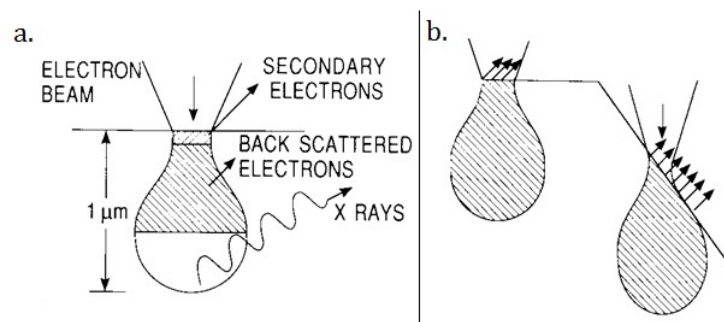


Figure A.5: a) Interaction volume showing the regions where different particles originate. b) Dependence of secondary electron yield on surface angle. [5]

Since different angles lead to different amounts of secondary electrons, the electron counts can be converted to brightness values on a computer, which result in a grayscale image of the sample surface. An electron microscope can achieve resolutions of the order of nanometers [5].

A.3 Energy-dispersive X-ray spectroscopy

Energy-dispersive X-ray spectroscopy (EDX) is a tool to determine the elemental content of a sample. It is based on the fact that each element has a unique X-ray spectrum. An excitation source (either electrons or X-rays) forms a beam that is focused on the sample. There, X-rays are emitted in the same way as for XRD (see Figure A.3). Using a detector, the energy and amount of the emitted X-rays can be measured. Since X-ray spectra are unique, the various peaks in an EDX measurement can then be attributed

to elements, determining the contents of the sample. Since a SEM setup naturally produces X-rays in this way, it is common to have an EDX module in such a setup [5].

A.4 References

- [1] Wikipedia, *Bragg's law*
http://en.wikipedia.org/wiki/Bragg_law, Retrieved: **29-05-2012**.
- [2] S.D. Marcum and J.M. Yarisson-Rice, *Bragg diffraction of X-rays and of electrons*, Miami University Ohio, **2000**.
- [3] Wikipedia, *Energy-dispersive X-ray spectroscopy*
http://en.wikipedia.org/wiki/Energy-dispersive_X-ray_spectroscopy, Retrieved: **29-05-2012**.
- [4] Wikipedia, *Scanning electron microscope*
http://en.wikipedia.org/wiki/Scanning_electron_microscope, Retrieved: **29-05-2012**.
- [5] M. Ohring, *Materials Science of Thin Films*, 2nd edition, Elsevier Inc., **2002**, .

B. Equipment

This section contains a list of equipment used during the experiments, what they were used for and, where applicable, references to images used in the text. Theoretical explanations of measuring equipment can be found in Appendix A.

Table B.1: Equipment used during the experiments

Name	Type	Images
Princeton Applied Research VersaSTAT 3	Potentiostat	
JEOL 5610	SEM	4.4, 4.7, 4.10
ZEISS 1550 equipped with NORAN EDS and WDS	High-resolution SEM, EDX	4.9, 4.3.d
Bruker D8	XRD	4.3.a, b and c, 4.5, 4.6, 4.8
Princeton Applied Research RDE0018 Analytical cell kit	Deposition cell, Reference electrode	
Vecstar Furnace	Annealing furnace	
Kern KB precision balance	Balance	
Branson 2200 ultrasonic cleaner	Ultrasonic bath	

C. Guide to electrodeposition

This guide will give a step-by-step explanation of how to do the electrodeposition as done in this bachelor project. The guide is divided into several steps:

- Preparing the bath
- Preparing the substrates
- Setting up the electrodeposition experiment
- After deposition

Due to the chemicals used in this experiment and to avoid dirt on the samples, wear gloves at all times when handling the substrate or chemicals.

C.1 Equipment

- Princeton Applied Research VersaSTAT 3. Software included: VersaStudio
- Ag/AgCl reference electrode with corresponding filling solution
- Deposition beaker (or cell), Princeton Applied Research Analytical Cell Kit (model RDE0018), which should be put into a larger holder.

C.2 Preparing a bath

The first thing to do is to measure the correct amount of materials for the solution. A balance is used for this (Kern KB in our case). The cell can hold a maximum of 120 mL of solution, but should ideally have around 100 mL. Place the cell close to the balance. This is done so that there is less risk of dropping material when putting it into the water. Using a small plastic cup (press the 'tare' button to set the balance back to 0 to account for the weight

of the cup), the amount of material needed can be measured, and any excess can be put back in the correct container. The material can then be put into the solution from the cup. Use a different spatula and cup for each material, or clean them before measuring another material.

After the correct amounts of material have been dissolved, a stir bar is added and then the bath needs to be stirred for around a half a day. The pH should be around 4-5 (to restrict movement and precipitation of H^+ ions), this can be checked using pH testers. Extra acid can be added if the pH is too high. Whenever the solution is not used, be sure to keep the stir bar stirring to avoid precipitation.

C.3 Preparing the substrates

Glass coated with a TCL (transparent conducting layer, in our case indium tin oxide, or ITO) is used as a substrate. The glass should be cut into pieces of around 20 mm by 10 mm, so that it fits in the sample box and fits through the cover of the deposition beaker. Before cutting the glass, cover the table with paper. Put some lens tissue on top of this. Lay the glass on the lens tissue with the TCL covered side towards the table. To measure which side is covered with TCL, use a multimeter in resistance mode. The TCL side should give a resistance (around 10 Ωcm for ITO), the other side is insulating.

When the glass lies on the table, use a diamond-cutter to apply a scratch. Then lay one side of the glass on a microscope glass with a piece of lens tissue in between (make sure the TCL side is on the paper). Press onto the other side to break the glass. It is essential that equal pressure is applied onto the other side, so that the glass breaks along the scratch. If unequal pressure is applied, there is a risk of getting small chips of glass or other cracks on the glass. To apply equal pressure, use another microscope glass to press on the other side.

C.4 Cleaning substrates

All the pieces of glass which have been cut should then be put in a beaker containing deionized water. Add excess detergent and put the beaker on a heater. The heater should be put to a temperature of around 120°C. Let the beaker rest on the heater for half a day. After half a day, the substrates should be cleaned in an ultrasonic bath (Branson 2200 in our case), using beakers each containing a different liquid (see Table C.1).

After the final treatment in the ultrasonic bath, the substrate should be put in a new beaker containing sufficient deionized water. If there will not

Table C.1: Chemicals used for cleaning substrates

Beaker contains	Time in ultrasonic bath	Notes
Deionized water	10 minutes	
Acetone	10 minutes	Use standard procedure for acetone waste
Isopropanol	10 minutes	Use standard procedure for isopropanol waste
Deionized water	10 minutes	

be any deposition for several days, cover the beaker to avoid letting it fall dry.

C.5 Setting up the deposition experiment

C.5.1 Reference electrode

With the deposition cell comes a Ag/AgCl reference electrode. When no deposition is being done, this electrode should be kept in a beaker containing a filling solution (saturated KCl-AgCl). This solution comes with the electrode. Always cover this beaker, to avoid letting the solution react with air. If the beaker is not covered, crystals will form in the solution. Before the electrode is put into the solution, it should be cleaned using deionized water. The reference electrode has a wire attached to it, which should be connected to the connector labeled 'RE' (see Figure C.1). The reference electrode should then be put into the solution.

**Figure C.1:** Connecting the Reference Electrode

C.5.2 Counter electrode

The counter electrode consists of a platinum sheet. When not doing deposition, this sheet should be kept in a beaker filled with deionized water. When setting up the experiment, use tweezers to grab the sheet and clean it with deionized water. The sheet should then be dried using a nitrogen gun. Use the clamp connector of the wire labeled 'CE' to attach the platinum sheet (see Figure C.2). Then put the sheet into the solution. The electrode should preferably stand vertical.



Figure C.2: Connecting the Counter Electrode

C.5.3 Working electrode

The working electrode is a shorter platinum sheet, with the substrate connected to it. This platinum sheet should be stored in the same beaker as the counter electrode. When setting up the experiment, the platinum sheet must be grabbed using tweezers, cleaned with deionized water and dry blown. Put the sheet aside somewhere close, since it is needed later. The next step is to take a glass substrate. Use tweezers to grab the very corner of the substrate. Dry the substrate using a nitrogen gun. Since the electrode should be conducting, the TCL covered side should be in contact with the platinum sheet. Use the multimeter to find out which side is conducting. Put the substrate onto the platinum sheet. Only a small part should be in contact with the sheet. Wind Teflon tape around the substrate and platinum sheet to combine the two. Use the multimeter again to check if the right side of the glass was connected to the platinum sheet. Now connect the platinum sheet to the wire labeled 'WE', by grabbing the sheet with the clamp (see Figure C.3). Now put the electrode into the cell, making sure only the uncovered part of the substrate is under the waterline. Make sure the conducting side faces

the counter electrode. The working electrode and counter electrode should preferably be parallel to each other.

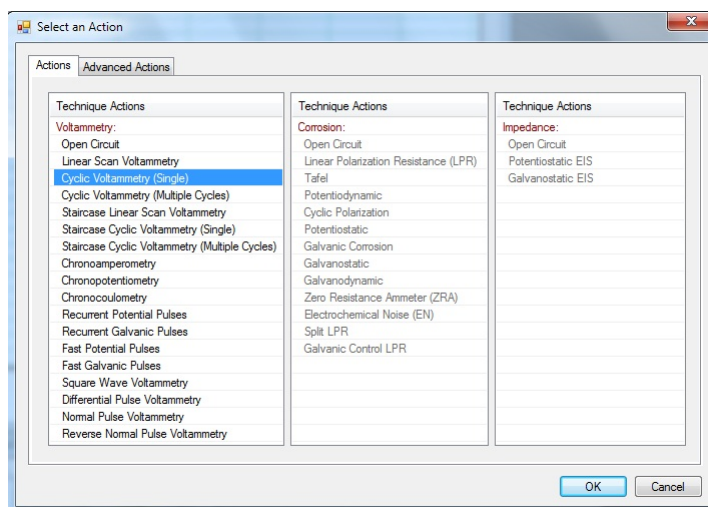


Figure C.3: Connecting the Working Electrode

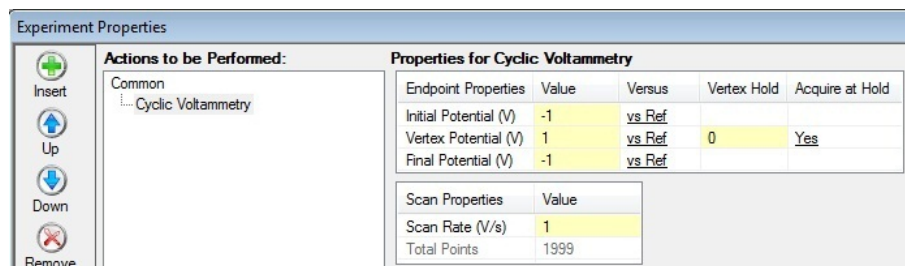
The next step is to start up the potentiostat. After turning the power on, one must wait around one minute before starting up the corresponding program, VersaStudio. VersaStudio is program used to do several electrochemical measurements.

C.5.4 New Bath

If a new bath is prepared, the first thing to do is a cyclic voltammetry (CV). Go to upper left corner → Experiment → New. A new screen will show up, from which one can select several experiments.



Select Cyclic Voltammetry (single) and click OK. Enter a filename and the data will automatically be saved. After pressing OK, the following screen will appear:



For CZTS, the following setup should be used:

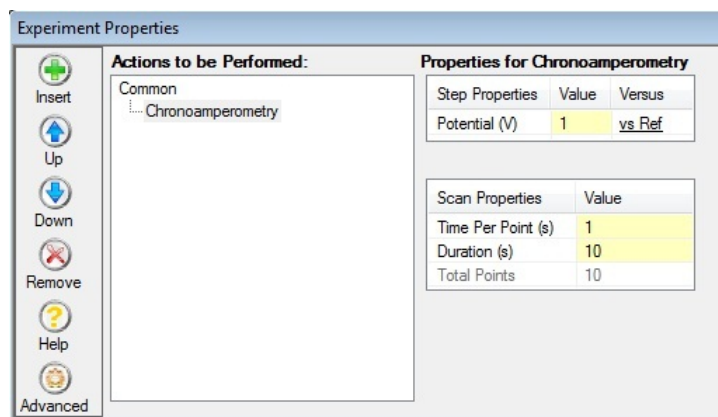
Initial potential	0 V
Vertex potential	-1.5 V
Final potential	0 V
Vertex Hold	0
Scan Rate	0.2 V/s

Then press the 'Run' button at the top of the screen.



The CV gives an indication of the reduction peak(s). Since CV is not ideal for non-reversible systems, the optimum potential has to be found experimentally, which should lie around the peak.

The next step is to clean the solution. To do this, deposition must be done at a potential which is more negative than one plans to use. This higher potential should remove any contaminations. After the first cleaning, the potential should be made less negative (in steps of around 0.1-0.15V). To start the actual cleaning, go to the upper left corner → Experiment → New. From the list of experiments, select chronoamperometry. A new screen will show up:



Select the potential (for depositing CZTS, this should always be negative) and the time. For cleaning the solution, a time of 5 to 10 minutes will suffice. **No or very low stirring should be applied during deposition.** Press the 'Run' button to start the experiment. Once the deposition experiment is completed, only the working electrode needs to be pulled from the solution. A new substrate must be attached to the platinum sheet, using the previously explained method. Once both the cyclic voltammetry and the cleaning of the solution have been done, it is best to let the solution rest for one day (with stirring), to make sure the materials have dissolved and mixed completely.

After this, deposition experiments can be started using the chronoamperometry mode, as explained earlier. When removing the substrate from the platinum sheet, it should be rinsed in a beaker containing deionized water. This is to check if the film is adhesive or contains powder. After rinsing, the film should be dry blown using the nitrogen gun. Use tweezers to handle the substrate. A small overview of the various beakers used in the experiment can be found in Table C.2.

Table C.2: Overview of the beakers

Beaker contains	Used for	Preferable size
Electrolyte	Contains materials to be deposited	Large
Deionized water 1	Storing platinum sheets	Large
Deionized water 2	Storing substrates	Large
Deionized water 3	Rinsing substrate after deposition	Small
KCl-AgCl filling solution	Storing reference electrode	Small

C.6 After the deposition experiment

Once the desired depositions have been done, the following steps should be undertaken. First close the VersaStudio program. Wait for one minute, before turning off the power to the VersaSTAT 3. The counter electrode can be put directly into the beaker containing the deionized water, where it was previously stored. For the working electrode, first the substrate needs to be removed from the platinum sheet. The platinum sheet can then be put in the same beaker containing the deionized water. The reference electrode should be cleaned very carefully using deionized water. No deposition solution should come into the beaker containing the filling solution. Cover the beakers containing the electrolyte and the filling solution.